RSC Advances

ROYAL SOCIETY OF CHEMISTRY

www.rsc.org/advances

Oxide-supported Rh catalysts for H_2 generation from low-temperature ethanol steam reforming: Effects of support, Rh precursor and Rh loading on catalytic performance

Lin Huang,* Catherine Choong, Luwei Chen, Zhan Wang, Ziyi Zhong, Kee Ann Chng[a] and Jianyi Lin*[b]

Institute of Chemical and Engineering Sciences, Agency for Science, Technology and Research, 1 Pesek Road, Jurong Island, Singapore 627833, Singapore

Fax: (+65)-6316-6182

E-mail: huang_lin@ices.a-star.edu.sg (L. Huang); LiJY@ntu.edu.sg (J. Lin)

[a] Present address: Ngee Ann Polytechnic, 535 Clementi Rd, Singapore 599489, Singapore

[b] Present address: Energy Research Institute @ NTU, Nanyang Technological University, 1 Cleantech Loop, Singapore 637141, Singapore

Abstract:

A variety of oxide-supported Rh catalysts prepared from frequently used oxides (γ-Al_2O_3, MgO, SiO_2, CeO_2, ZrO_2, La_2O_3, Y_2O_3,TiO_2 and ZnO) and Rh compounds ($Rh(NO_3)_3 \cdot xH_2O$, $RhCl_3 \cdot xH_2O$, $Rh(acac)_3$ and $Rh_4(CO)_{12}$) for H_2 generation from ethanol steam reforming (ESR) at low temperatures (250-400 ^oC) have been studied. Catalytic screening shows that Rh/CeO_2 is advantageous over other frequently used oxide-supported Rh catalysts. Rh/CeO_2 behaves as the most effective catalyst for the water gas shift (WGS) pathway during ESR. Combination of CeO_2 and $Rh_4(CO)_{12}$ with a 1 % Rh loading results in an optimal-performance catalyst that brings about a CO-free H_2 yield of 4 mol/mol C_2H_5OH at 350 ^oC with good catalytic stability. Comparison of thermodynamic and catalytic data of ESR indicates that low-temperature ESR is strongly kinetically controlled over Rh/CeO_2 in favour of H_2 production via the acetaldehyde steam reforming, acetaldehyde decarbonylation, steam reforming of adsorbed CH_x (x = 1-3) and WGS pathways. Combined studies by catalytic stability, thermogravimetric analysis, X-ray photoelectron spectroscopy, transmission electron microscopy and X-ray diffraction suggest that the catalytic stability of Rh/CeO_2 is markedly affected by coking which is the only cause of catalyst deactivation during low-temperature ESR and that both CeO_2-supported Rh^0 and Rh^+ are the active sites for ESR to produce H_2. The effects of support, Rh precursor, Rh loading and calcination of precatalyst on the catalytic performance are discussed. In addition, catalytic roles played by typical oxides in reaction pathways during ESR are elucidated.

Introduction

The ethanol steam reforming (ESR) process yields pure H_2 and CO_2 only under ideal conditions, and inevitably produces CO and CH_4 as the main undesirable products under usual conditions. Thermodynamically, ESR is strongly endothermic.[1] High temperatures are beneficial to direct C_2H_5OH conversion to H_2, methane steam reforming (MSR) to H_2 and decoking. At the same time, high temperatures are detrimental to water gas shift (WGS), reverse WGS takes off to produce CO and lower H_2 yield. On the contrary, low temperatures are favourable to WGS, methanation and coking. Because of the high demand for low-temperature ESR that meets the needs of applications, low-temperature ESR is facing challenges of effciency of H_2 production and formation of undesirable products. Although thermodynamic considerations are substantial, kinetic control of ESR in favour of a high H_2 yield and low yields of undesirable products is more important. Under identical thermodynamic conditions, a dozen of studies mostly on high temperature ESR clearly indicated that distinct yields of H_2 and distributions of products (H_2, CH_4, CO, CO_2, C_2H_4, C_2H_6, CH_3CHO and coke, etc.) could be obtained with diverse types of catalysts.[2-7] Furthermore, Auprêtre et al. reported that in the presence of 1 %Rh/γ-Al_2O_3 or 9.7 %Ni/γ-Al_2O_3 at 600 ^oC, the selectivity to H_2 was obviously higher than the thermodynamic equilibrium value while the selectivities to CO and to CH_4 were greatly lower than the thermodynamic equilibrium values.[8] Roh et al. found that in the presence of 1 %Rh/ZrO_2-CeO_2 at 450 ^oC, the H_2 yield significantly surpassed the thermodynamic equilibrium value.[4] Rossi et al., who compared their thermodynamic analyses with experimental results reported by others over the supported metal catalysts Rh/γ-Al_2O_3,[9] Ni/MgO[10] and Ni/γ-Al_2O_3[11-13] at 500-800 ^oC, noticed that the selectivity values to H_2 over these catalysts were significantly higher than those calculated by their proposed methodology for high-temperature ESR.[14] Such results illuminate that ESR is kinetically controlled under normal reaction conditions. Hence, it can be expected to control the kinetics of ESR through appropriate catalysts at low temperatures and thus increase the selectivity to H_2 against undesirable products.

The catalytic ESR reaction for the production of H_2 has been extensively studied with supported transition metal and Cu catalysts.[2,15-17] Catalytic activity, selectivity (or product distribution) and stability during ESR are virtually dependent on the nature of the metal and support and the metal-support interaction. Towards H_2 production from steam reforming reactions with supported metal catalysts, it was admitted that the supports more or less play a real catalytic role[18-22] whereas the metals may function as promoters of supports.[6] On the other hand, Homs's group demonstrated that the mixture of Co^0 and CoO derived from bulk Co_3O_4 is active and selective for H_2 production from ESR,[23,24] which hinted that the Co metal alone may be the true catalyst. Very recently, the evidence that the metals alone can independently

fulfill H_2 production from ESR was reported by Divins et al., working with Rh-Pd bimetallic nanoparticles.[25] They meanwhile demonstrated with CeO_2-supported Rh-Pd bimetallic nanoparticles that the support can play not only an important catalytic role through new active sites but also a pivotal promotional role via the metal-support interaction in ESR.[25] The new understanding of the activation of C_2H_5OH and H_2O on the surfaces of metal particles and supports has been summarized by several recent reviews.[26-30] The support, nature of the metal, metal particle size and metal oxidation state determine the reaction pathways. A better understanding of the reaction mechanism and the influence of these factors on the reaction pathways should lead toward the development of high performance supported metal catalysts for ESR.

Over supported metal catalysts, ESR would follow a bifunctional mechanism where C_2H_5OH is activated on the metal particles while H_2O is activated mainly on the supports.[29] On the metal particles, C_2H_5OH is adsorbed as surface ethoxy or oxametallacycle, which favours the C-C bond cleavage. On the supports, H_2O is adsorbed as surface OH, which facilitates steam reforming of different surface species. The supports may serve to promote migration of surface OH towards the metal particles for steam reforming and stabilization of the metal particles. In addition, the metal-support interaction, an indispensable factor determining the catalytic properties, should be considered.[29,31] It is envisioned that ESR primarily occurs in a bifunctional manner on both the dispersed metal particles and the support and that most of the activity is at the metal-support interface. The catalytic properties may be dependent on the nature of the interaction between the metal particles and the support.

A complex ESR reaction system may consist of primary reactions and secondary reactions. Herein, the primary reactions refer to C_2H_5OH reactions that give primary products, as depicted below:

Ethanol dehydrogenation to acetaldehyde (EDA): $C_2H_5OH \rightarrow CH_3CHO + H_2$ (1)

Ethanol decomposition to acetone (EDAC): $2C_2H_5OH \rightarrow (CH_3)_2CO + CO + 3H_2$ (2)

Ethanol dehydration to ethylene (EDE): $C_2H_5OH \rightarrow C_2H_4 + H_2O$ (3)

Ethanol dehydrogenation to adsorbed oxametallacycle: $C_2H_5OH \rightarrow CH_2CH_2O(ads) + H_2$ (4)

The secondary reactions implicate further reactions of primary products, as represented below:

Adsorbed oxametallacycle decarbonylation: $CH_2CH_2O(ads) \rightarrow CH_4 + CO$ (5)

Acetaldehyde steam reforming (ASR): $CH_3CHO + H_2O \rightarrow 2CO + 3H_2$ (6)

Acetaldehyde decarbonylation (AD): $CH_3CHO \rightarrow CH_4 + CO$ (7)

Acetaldehyde oxidation to adsorbed acetate: $CH_3CHO + OH(ads) \rightarrow CH_3COO(ads) + H_2$ (8)

Acetone steam reforming (ACSR): $(CH_3)_2CO + 2H_2O \rightarrow 5H_2 + 3CO$ (9)

Adsorbed ethoxy oxidation to adsorbed acetate: $C_2H_5O(ads) + H_2O \rightarrow CH_3COO(ads) + 2H_2$ (10)

Adsorbed acetate decomposition to methane and carbon dioxide:

$CH_3COO(ads) + OH(ads) \rightarrow CH_4 + CO_2 + O(ads)$ (11)

WGS: $CO + H_2O \rightarrow CO_2 + H_2$ (12)

Reverse WGS: $CO_2 + H_2 \rightarrow CO + H_2O$ (13)

Carbon monoxide methanation: $CO + 3H_2 \rightarrow CH_4 + H_2O$ (14)

Carbon dioxide methanation: $CO_2 + 4H_2 \rightarrow CH_4 + 2H_2O$ (15)

MSR: $CH_4 + H_2O \rightarrow CO + 3H_2$ (16)

Methane decomposition (MD): $CH_4 \rightarrow 2H_2 + C$ (17)

Ethylene steam reforming (Ethylene SR): $C_2H_4 + 2H_2O \rightarrow 2CO + 4H_2$ (18)

Ethylene decomposition (ED): $C_2H_4 \rightarrow 2H_2 + 2C$ (19)

Boudouard reaction (BR): $2CO \rightarrow CO_2 + C$ (20)

In usual cases, reforming catalysts merely allow yielding finite H_2 with the concurrent production of CO, CH_4 and CO_2, etc. If a high yield of H_2 is required with the minimal formation of CO and CH_4, development of catalysts containing effective components for the secondary reactions must be considered. Quite a number of studies have been reviewed concerning integrated functional ESR catalysts allowing for both primary and secondary reactions in view of activity, selectivity and stability.[2,15-17] Bicomponent metals such as Cu+Ni, Rh+Pt, Rh+Pd, Rh+Ni, Rh+Fe and Rh+Co are apt to not only ensure dissociation of the C-C bond but also improve efficiency of WGS and coke tolerance of catalysts.[25,32-40] Alkaline metals such as K, Li, Na and Ca are able to neutralize acid sites of supports and thus reduce coke formation.[32,38,41-44] Basic and redox oxides like MgO, ZnO, V_2O_5, CeO_2 and CeO_2-ZrO_2 as supports are suitable to promote EDA and/or WGS.[4,18,20,21,45,46] Use of CeO_2 permits diminution of coke formation.[47-50] CeO_2 and CeO_2-ZrO_2 have the ability to promote CO oxidation.[51-53] CeO_2-ZrO_2 is also helpful to MSR to H_2.[54]

Previous studies have shown that Rh catalysts are more active than other metal catalysts for H_2 generation from ESR.[3,8,9,22,43,55,56] Although numerous catalytic investigations of oxide-supported Rh catalysts in ESR have been undertaken,[2-4,9,41,55-69] few papers have been published on the comparative study of different types of oxide-supported Rh catalysts.[8,58,63,70] Moreover, almost all these catalytic data published are restricted to ESR at high temperatures (above 400 ^oC). The present paper reports comparative work on various types of oxide-supported Rh catalysts for H_2 generation from ESR at 250-400 ^oC. In our work, we systematically examined the catalytic properties of typical oxides such as γ-Al_2O_3, MgO, SiO_2 and CeO_2, as well as Rh supported on various types of oxides including γ-Al_2O_3, MgO, SiO_2, CeO_2, ZrO_2, La_2O_3, Y_2O_3,TiO_2 and ZnO in low-temperature ESR, in order to illustrate the roles of Rh and the various types of oxides in low-temperature ESR. Through a screening of these oxide-supported Rh catalysts, an optimal combination between Rh precursors and supports was reached. By

comparing the catalytic performances of Rh/CeO_2 at different Rh loadings, the effect of dispersion of Rh metal on H_2 generation from ESR was demonstrated. To learn about the reductive behaviour of the Rh precatalysts and the Rh-support interaction, we performed a temperature-programmed reduction (TPR) investigation on all the Rh precatalysts studied. To shed light on the causes of deactivation of Rh catalysts during ESR, we conducted a series of analyses including thermogravimetric analysis (TGA), X-ray photoelectron spectroscopy (XPS), transmission electron microscopy (TEM) and X-ray diffraction (XRD) on Rh/CeO_2. In addition, the influence of strong Rh-support interaction on H_2 generation from ESR and the kinetic control of H_2 generation from ESR with Rh/CeO_2 were discussed.

Results and discussion

Behaviour of catalysts in ESR

Typical oxides and their respective oxide-supported Rh catalysts Figs. 1-4 illustrate the overall catalytic results of most frequently used oxides (γ-Al_2O_3, MgO, SiO_2 and CeO_2) and their respective oxide-supported Rh catalysts prepared from $Rh(NO_3)_3 \cdot xH_2O$ in ESR. In the case of the acidic oxide γ-Al_2O_3 (Fig. 1), γ-Al_2O_3 alone brought about only a C_2H_5OH conversion of 0.7 % and a negligible H_2 yield at 250 ^oC. At this temperature, CH_3CHO (76.6 % S) and C_2H_4 (23.3 % S) were also detected. The results suggest that EDA occurs as the major primary reaction with the concomitant EDE as the minor primary reaction at lower temperatures over γ-Al_2O_3, consistent with the dominant formation of CH_3CHO in a C_2H_5OH oxidation reaction over Al_2O_3 at 227 ^oC reported earlier.[71] From 250 to 300 ^oC, the selectivity to CH_3CHO dramatically dropped to 14.4 % with concurrent quick rise to 85.6 % in the selectivity to C_2H_4 as the C_2H_5OH conversion increased. From 300 ^oC onwards, a rapid increase was noted in the C_2H_5OH conversion, which reached 78.4 % at 400 ^oC. Meanwhile, only trace amounts of H_2 were detected at 400 ^oC. This demonstrates that C_2H_5OH is mostly converted to C_2H_4 via EDE as a primary reaction once the C_2H_5OH decomposition proceeds at higher temperatures over γ-Al_2O_3, in agreement with reported product distributions of ESR and C_2H_5OH oxidation over Al_2O_3 at 427-450 ^oC.[21,71,72] Above 400 ^oC, C_2H_5OH was quickly fully converted and H_2 gradually rose with increasing temperature. An H_2 yield of 1.35 mol/mol C_2H_5OH was obtained at 600 ^oC. The selectivity to C_2H_4 rose to 94.5 % at 500 ^oC but fell to 87.6 % at 600 ^oC. The selectivity to CH_3CHO fell progressively to 0.6 % at 600 ^oC. From the variations of selectivities to CH_3CHO, C_2H_4 and H_2 at 400-600 ^oC, H_2 appears to arise as a secondary product from ED instead of AD and ethylene SR. $Rh(N)/\gamma$-Al_2O_3 already had a fairly good activity at 250 ^oC, which enabled conversion of C_2H_5OH at 64.7 %, concomitant with an H_2 yield at 1.76 mol/mol C_2H_5OH. At the same time, CH_3CHO (19.1 % S), CH_4 (34.8 % S) and CO (45.5 % S) were produced. This shows that the

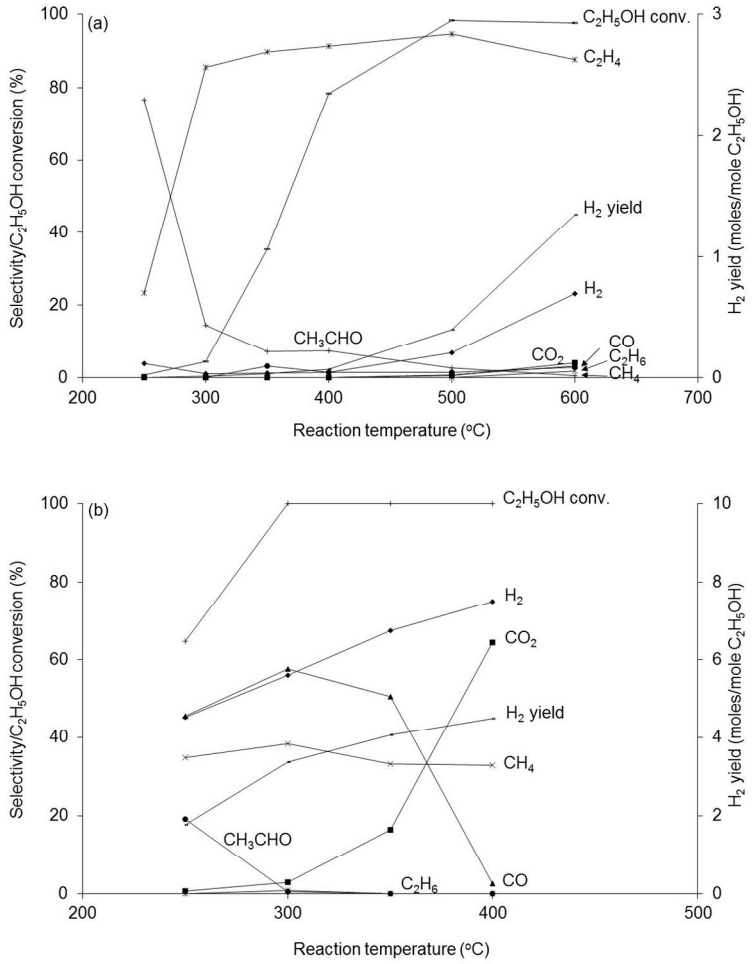

Fig. 1 Catalytic properties of (a) γ-Al_2O_3 and (b) Rh(N)/γ-Al_2O_3 as a function of reaction temperature.

Rh obviously catalyzes not only EDA but also ASR and AD. At 300 °C, the conversions of C_2H_5OH and CH_3CHO were complete, the selectivities to CH_4 and CO started to fall in favour of the rise in the selectivities to H_2 and CO_2, evidently due to the occurrence of MD and WGS. At 400 °C, the H_2 yield attained to 4.5 mol/mol C_2H_5OH with the nearly complete removal of CO. Throughout the ESR process over Rh(N)/γ-Al_2O_3, no C_2H_4 was detected, probably because of predominant EDA over EDE by competition in the presence of the Rh.

In the case of the basic oxide MgO (Fig. 2), MgO alone did not produce a C_2H_5OH conversion of 4.9 % with trace amounts of H_2 until 400 °C. Besides, a selectivity to CH_3CHO of 100 % at 400 °C and below indicates that only a rather slow EDA occurs as a primary reaction over MgO at low temperatures. Above 400 °C, the C_2H_5OH conversion increased rapidly, the selectivity to CH_3CHO decreased progressively with the concurrent slight increase in the selectivity to C_2H_4. At 600 °C, 85.0 % of C_2H_5OH was converted mainly to CH_3CHO (78.0 % S), C_2H_4 (12.7 % S), CO_2 (5.9 % S), CO (1.5 % S), CH_4 (1.9 %

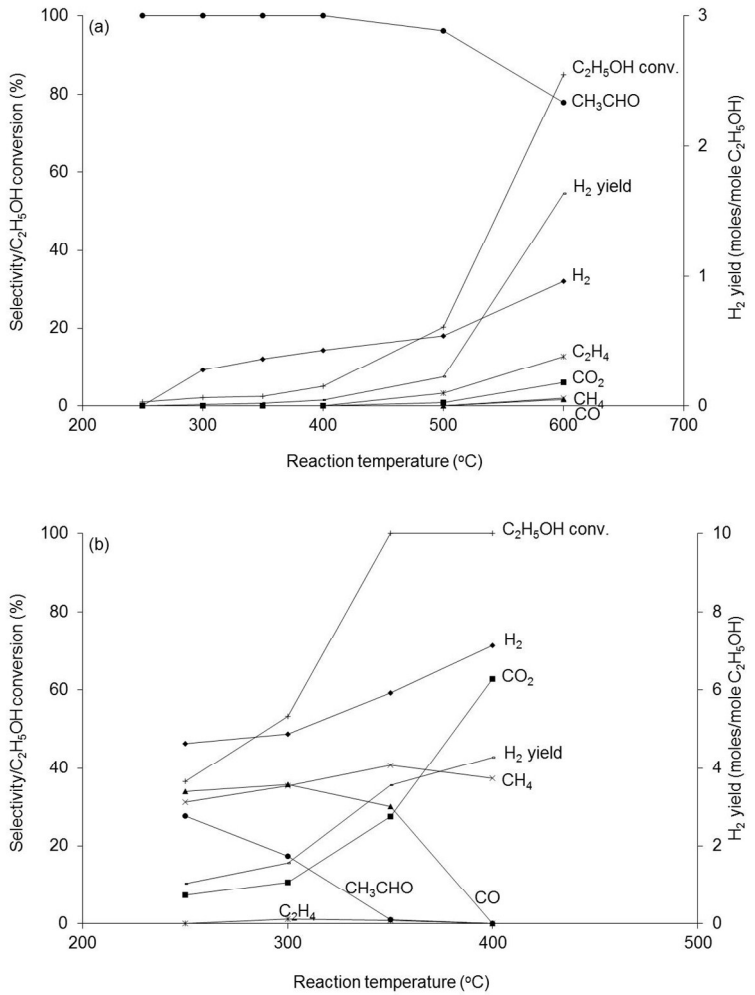

Fig. 2 Catalytic properties of (a) MgO and (b) Rh(N)/MgO as a function of reaction temperature.

S) and H_2 (32.1 % S). This suggests that EDA still dominates the reaction pathways over MgO at high temperatures, in accordance with reported product distributions of ESR and C_2H_5OH oxidation over MgO at 227-450 °C.[21,71] The H_2 yield was low, being just 1.64 mol/mol C_2H_5OH. Only a small part of H_2 may arise from ASR followed by WGS, since MgO is known as a catalyst for WGS.[73,74] Over Rh(N)/MgO, 36.6 % of C_2H_5OH was already converted, concomitant with an H_2 yield of 1.02 mol/mol C_2H_5OH at 250 °C, at which CH_3CHO (27.6 % S), CH_4 (31.3 % S), CO (33.9 % S) and CO_2 (7.2 % S) were observed as well. We infer from the general evolutions of CH_3CHO, CO, CO_2 and H_2 that the Rh promotes WGS besides EDA, ASR and AD. At 350 °C, C_2H_5OH was completely converted and CH_3CHO nearly disappeared. From 300 to 350 °C, the selectivities to CH_4, CO_2 and H_2 rose at the expense of the selectivities to CH_3CHO and CO, which may be indicative of the occurrence of ASR, AD and WGS. At 400 °C, the H_2 yield attained to 4.28 mol/mol C_2H_5OH. The selectivities to CO and CH_4 fell with the concomitant increase in the selectivities to CO_2 and H_2. Based on the variations of selectivities to the

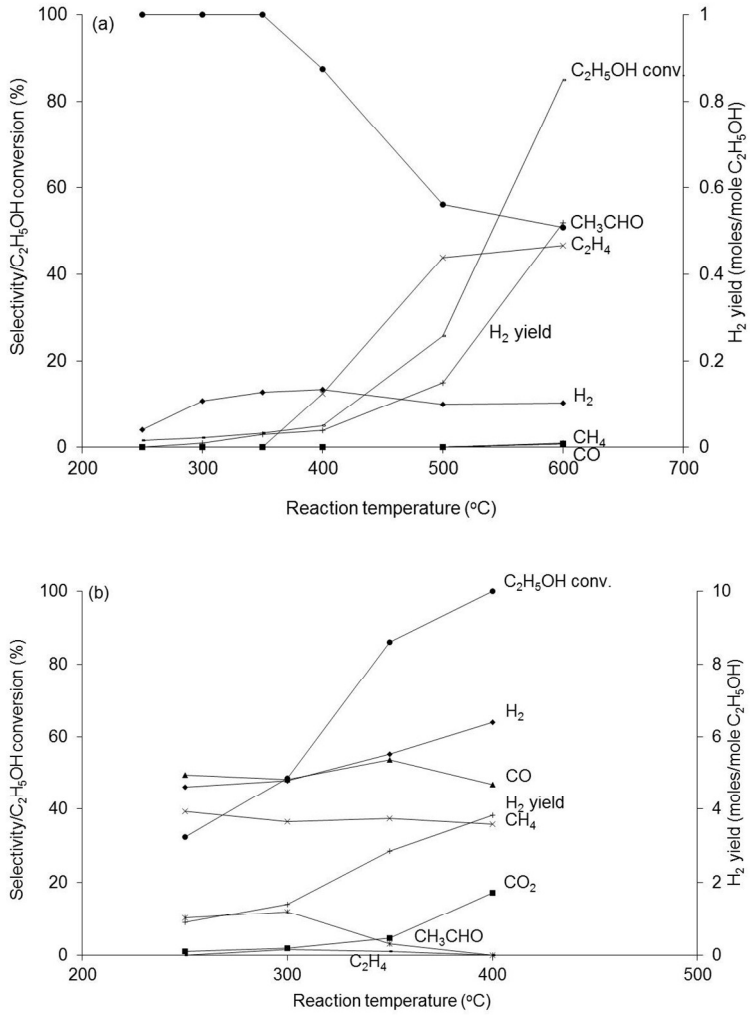

Fig. 3 Catalytic properties of (a) SiO_2 and (b) Rh(N)/SiO_2 as a function of reaction temperature.

products from 350 to 400 °C, we infer that MD, WGS and BR take place to give H_2, CO_2 and coke at 400 °C. Throughout the ESR process over Rh(N)/MgO, limited CH_3CHO was observed, likely because ASR and AD proceed quickly in the presence of the Rh.

In the case of the weakly acidic oxide SiO_2 (Fig. 3), SiO_2 alone did not bring about a C_2H_5OH conversion of 3.3 % until 350 °C, at which only 0.03 mol H_2/mol C_2H_5OH was produced together with CH_3CHO (100 % S). At 250-350 °C, only CH_3CHO and H_2 were detected as products, suggesting that EDA takes place as a primary reaction over weakly acidic oxides like SiO_2 in low speed at lower temperatures. Above 350 °C, the selectivity to C_2H_4 ascended with the concurrent fall in the selectivity to CH_3CHO, as the C_2H_5OH conversion ascended. At 600 °C, 85.0 % of C_2H_5OH was converted mainly to CH_3CHO (50.8 % S), C_2H_4 (46.6 % S) and H_2 (10.3 % S). The results indicate that both EDA and EDE occur as primary reactions over weakly acidic oxides like SiO_2 at higher temperatures. Increasing the

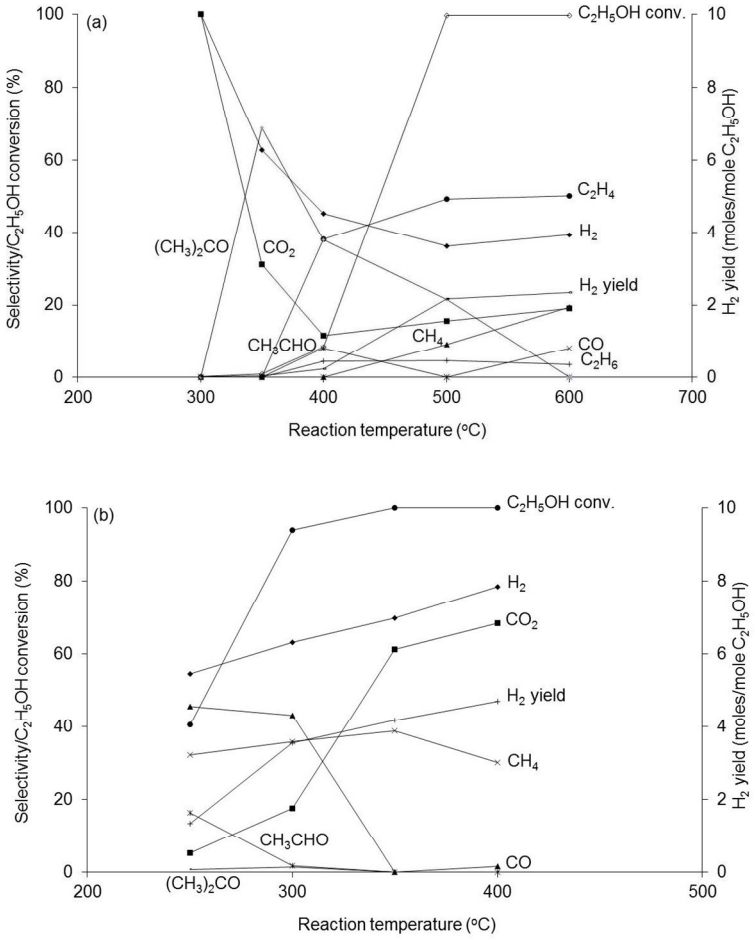

Fig. 4 Catalytic properties of (a) CeO_2 and (b) Rh(N)/CeO_2 as a function of reaction temperature.

temperature increases the rate of EDE relative to EDA in competition over SiO_2. Possibly due to both the weak acidity and basicity of SiO_2,[75] its activity for EDE is incomparable to that of γ-Al_2O_3 and its activity for EDA is lower than that of MgO based on this work. At 600 °C, the H_2 yield came to only 0.52 mol/mol C_2H_5OH. It is thus inferred that H_2 results from EDA rather than other reaction pathways, in accordance with what was noted by Carrero et al. in ESR over silicate SBA-15.[76] Rh(N)/SiO_2 was active enough to totally convert C_2H_5OH with the production of 3.83 mol H_2/mol C_2H_5OH at 400 °C, suggesting strong catalysis or promotion by the Rh. From 250 to 400 °C, a low selectivity to CH_3CHO was accompanied by high selectivities to CH_4, CO and H_2, hinting that the primary product from EDA is rapidly transfomed to the secondary products via ASR and AD in the presence of the Rh. From 350 to 400 °C, the selectivity to CO fell slightly in favour of the rise in the selectivities to both CO_2 and H_2, indicating the occurrence of WGS. During the ESR process over Rh(N)/SiO_2, only trace amounts of C_2H_4 were discerned, probably because EDA dominates over EDE by competition in the presence of the Rh.

In the case of the redox oxide CeO_2 (Fig. 4), CeO_2 alone gave rise to a C_2H_5OH conversion of 0.1 %

with high selectivities to H_2 and CO_2 at 300 ^oC. This may imply that C_2H_5OH decomposition occurs in low speed followed by steam reforming and WGS in high speed at lower temperatures. At 350 ^oC, $(CH_3)_2CO$ was produced as a primary product in a selectivity as high as 68.8 % concomitant with H_2 (62.7 % S) and CO_2 (31.1 % S). This signifies that $(CH_3)_2CO$ is an important reaction intermediate and that both EDAC and WGS are accelerated at 350 ^oC. The C_2H_5OH conversion did not come to 8.4 % until 400 ^oC, at which CH_3CHO (8.0 % S) and just 0.23 mol H_2/mol C_2H_5OH were produced together with $(CH_3)_2CO$ (38.0 % S), C_2H_4 (38.1 % S), C_2H_6 (4.4 % S) and CO_2 (11.5 % S), indicating that EDA, ASR, EDAC, ACSR, EDE and WGS take place simultaneously. At 500 ^oC, the C_2H_5OH conversion was full and the H_2 yield was as high as 2.16 mol/mol C_2H_5OH. In addition, $(CH_3)_2CO$ (21.5 % S), C_2H_4 (49.3 % S), C_2H_6 (4.6 % S), CH_4 (9.0 % S) and CO_2 (15.6 % S) were observed with the disappearance of CH_3CHO, indicating that AD and/or acetone decomposition (ACD) take place besides ASR, ACSR, EDE and WGS. At 600 ^oC, $(CH_3)_2CO$ disappeared with the concurrent appearance of CO and slight rise in the selectivities to H_2 and CO_2. Meanwhile, the selectivity to CH_4 continued to rise and the selectivity to C_2H_4 remained almost unchanged. This means that while $(CH_3)_2CO$ transformation proceeds, WGS may slow down at 600 ^oC. The overall observations during ESR over CeO_2 postulate that EDE takes place and becomes more important than EDA from 400 ^oC onwards. Possibly because of the weak acidity of CeO_2,[75] its activity for EDE is much lower than that of γ-Al_2O_3. However, the activities of CeO_2 for EDA and EDAC are fairly high despite the weak basicity of CeO_2.[75] This may be explained by strong catalysis by CeO_2 for CH_3CHO transformation (ASR and AD), $(CH_3)_2CO$ transformation (ACSR and ACD) and WGS, which stimulates the chemical equilibrium shifts of EDA and EDAC. The observed higher selectivity to $(CH_3)_2CO$ at 350-500 ^oC is in accordance with reported product distributions of ESR over CeO_2 at 400-450 ^oC.[21,72] The obvious observation of CO_2 should be an indication of the efficient occurrence of WGS over CeO_2, since CeO_2 is known as an effective catalyst for WGS.[18-20] Over Rh(N)/CeO_2, 40.6 % of C_2H_5OH was converted and 1.33 mol H_2/mol C_2H_5OH was produced together with CH_3CHO (16.3 % S), $(CH_3)_2CO$ (0.6 % S), CH_4 (32.3 % S), CO_2 (5.1 % S) and CO (45.7 % S) at 250 ^oC. The formation of $(CH_3)_2CO$ suggests a promoting effect of the Rh on EDAC occurring over CeO_2, although Rh alone is unable to catalyze the EDAC pathway in C_2H_5OH reactions.[77-79] Above 250 ^oC, the selectivity to CO declined in favour of the rise in the selectivities to CO_2 and H_2. At 350 ^oC, C_2H_5OH was fully converted and the H_2 yield continued to rise. CH_3CHO, $(CH_3)_2CO$ and CO vanished with the concomitant enhancements of CH_4, CO_2 and H_2. The results imply that the Rh effectively promotes WGS in addition to EDA, EDCA, ASR, AD, ACSR and ACD. At 400 ^oC, the H_2 yield went up to 4.70 mol/mol C_2H_5OH. The selectivity to CH_4 declined markedly together with the appearance of small amounts of CO and a marked increase in the selectivity to CO_2. The transformation of CH_4 may go via MD and steam

Table 1 Properties of typical oxide-supported Rh catalysts in ESR[a]

catalyst	T (°C)	C_2H_5OH conv %	H_2 yield (mol/mol C_2H_5OH)	selectivity %							$S(CO_2)/S(CO)$	$S(CO_2)//S(H_2)$
				H_2	CO_2	C_2H_4	C_2H_6	CH_4	CO	CH_3CHO		
Rh(N)/γ-Al_2O_3	250	64.7	1.76	45.3	0.6	0	0	34.8	45.5	19.1	0.01	0.01
	300	100	3.37	38.3	2.8	0	0.7	56.1	57.7	0.5	0.05	0.05
	350	100	4.05	67.5	16.4	0	0	33.1	50.5	0	0.33	0.24
	400	100	4.50	75.0	64.5	0	0	32.9	2.6	0	24.6	0.86
Rh(N)/MgO	250	36.5	1.02	31.3	7.2	0	0	46.3	33.9	27.6	0.21	0.16
	300	53.3	1.56	48.8	10.6	1	0	35.4	35.7	17.3	0.30	0.22
	350	100	3.56	59.3	27.5	0.7	0	40.8	30.	0.90	0.92	0.47
	400	100	4.28	71.3	62.8	0	0	37.3	0	0	–	0.88
Rh(N)/SiO_2	250	32.4	0.90	46.1	1.0	0	0	39.3	49.5	10.2	0.02	0.02
	300	48.6	1.40	48.0	1.8	1.5	0	36.6	48.2	11.9	0.02	0.02
	350	86.2	2.86	55.3	4.7	1.0	0	37.5	53.7	3.1	0.06	0.06
	400	100	3.83	63.9	17.2	0	0.1	35.8	46.9	0	0.37	0.27
Rh(N)/CeO_2[b]	250	40.9	1.35	55.2	5.6	0	0	32.9	45.5	16.0	0.12	0.10
	300	94.1	3.60	63.8	19.1	0	0.2	36.3	42.7	1.7	0.45	0.30
	350	100	4.18	69.7	61.2	0	0	38.8	0	0	–	0.88
	400	100	4.70	78.4	68.4	0	0	30.1	1.5	0	42.6	0.87

[a] 0.15 g of precatalyst, 1 % Rh loading in precatalysts, Ar : C_2H_5OH : H_2O = 49 : 1 : 10 molar ratio, gas phase hourly space velocity (GHSV) = 26200/h, data taken 20 min later after initiation of reaction at each reaction temperature. [b] Excluding trace $(CH_3)_2CO$ at 250 and 300 °C.

reforming of adsorbed CH_x (x = 1-3) followed by WGS to give H_2, CO and CO_2. During the ESR process over Rh(N)/CeO_2, C_2H_4 was not detected, probably owing to predominant EDA and EDAC over EDE by competition in the presence of the Rh. Trace $(CH_3)_2CO$ ($S \leq 1.4$ %) was detected only at 250 and 300 °C, probably because of predominant $(CH_3)_2CO$ transformation over EDAC by competition in the presence of the Rh.

Overall, all these four typical oxides themselves are able to catalyze the ESR process to generate H_2 to a different extent, though the H_2 yield is very low compared to supported metal catalysts. The acidic oxide γ-Al_2O_3 favours EDE followed by ED, the basic oxide MgO benefits EDA, the weakly acidic oxide SiO_2 catalyzes EDA to a small extent, and the redox oxide CeO_2 eases WGS following ASR, AD, ACSR and ACD. Towards C_2H_5OH decomposition over these oxides, the reaction pathways are likely related to the acid-base properties of oxide surfaces. The rates of EDE and EDA (or EDA plus EDAC) are likely dependent on the acidity and basicity of oxides, respectively. The rates of EDA and EDAC rely also on the redox property of the oxides. The relative rate between EDE and EDA over an oxide may basically rely on both the acidity and basicity of the oxide. The order of the catalyst activity for EDE can be ranked as γ-Al_2O_3 > CeO_2 > SiO_2 > MgO, while the order for EDA (or EDA plus EDAC) can be ranked as CeO_2 > MgO > SiO_2 > γ-Al_2O_3. The presence of Rh on these oxides leads to strong catalysis or substantial promotion for all the reaction pathways as a whole, since H_2 production from ESR over oxide-supported metal catalysts is realized through the metal-oxide concerted action.[25,29] In the presence of Rh on these oxides, EDA (or EDA plus EDAC) dominates over EDE as a primary reaction pathway.

Table 1 summarizes the catalytic properties of the four Rh(N)/oxide catalysts in ESR at 250-400 °C. Rh(N)/CeO_2 performs better, producing a higher H_2 yield than the other three Rh(N)/oxide catalysts at 250-400 °C, except a lower H_2 yield than Rh(N)/γ-Al_2O_3 at 250 °C. The order of the catalyst activity for

H_2 production can be generally ranked as Rh(N)/CeO_2 > Rh(N)/γ-Al_2O_3 > Rh(N)/MgO > Rh(N)/SiO_2. Rh(N)/γ-Al_2O_3 is more active than the others for EDA (or EDA plus EDAC) at all the temperatures, and for CH_3CHO transformation at 300-400 ^oC. The order of the catalyst activity for EDA (or EDA plus EDAC) can be ranked as Rh(N)/γ-Al_2O_3 > Rh(N)/CeO_2 > Rh(N)/MgO > Rh(N)/SiO_2, while the order for CH_3CHO transformation at 300-400 ^oC can be ranked as Rh(N)/γ-Al_2O_3 > Rh(N)/CeO_2 > Rh(N)/MgO > Rh(N)/SiO_2. However, the residual amounts of CO and CH_4 in the reforming products vary with the catalyst selectivity to the secondary reactions. Over all these catalysts, CH_3CHO is transformed to CH_4, CO and H_2 via AD and ASR. Over Rh(N)/CeO_2, $(CH_3)_2CO$ may be converted to CH_4, H_2, CO and CO_2 via ACSR and ACD.[80-82] CO is further converted to H_2 via WGS to a different extend, whereas CH_4 is transformed to H_2 via MD or steam reforming of adsorbed CH_x (x = 1-3) to a limited extend as the high selectivities of 30.1-37.3 % at 400 ^oC are obtained. Among all these catalysts, Rh(N)/CeO_2 is most active and Rh(N)/SiO_2 least active for CH_4 transformation to H_2. The S(CO_2)/S(CO) value can represent the ability of Rh(N)/oxide to catalyze WGS in ESR, and the S(CO_2)/S(H_2) value can reflect the contribution of WGS to the total production of H_2 in ESR, assuming that BR is unimportant. In the whole temperature range, both the S(CO_2)/S(CO) and the S(CO_2)/S(H_2) values increase substantially as the reaction temperature increases for all the four catalysts, signifying that both the activity for WGS and the contribution of WGS to the total production of H_2 increase generally with increasing temperature. It is evident that the orders of the average catalyst activity for WGS at 250-400 ^oC and the catalyst activity for WGS at 300 and 350 ^oC are ranked as Rh(N)/CeO_2 > Rh(N)/MgO > Rh(N)/γ-Al_2O_3 > Rh(N)/SiO_2. This order matches with those of the average contribution of WGS to the total production of H_2 at 250-400 ^oC and the contribution of WGS to the total production of H_2 at 300 and 350 ^oC. On the other hand, the S(CO_2)/S(CO) maximum corresponds to the minimum of remaining CO in ESR, and the S(CO_2)/S(H_2) maximum means the maximal contribution of WGS to the total production of H_2 in ESR. From Table 1, the S(CO_2)/S(CO) maxima for Rh(N)/SiO_2, Rh(N)/γ-Al_2O_3, Rh(N)/MgO and Rh(N)/CeO_2 correspond to the selectivities to CO of 28.6 at 400 ^oC, 1.5 at 400 ^oC, 0 at 400 ^oC and 0 at 350 ^oC, respectively. The corresponding S(CO_2)/S(H_2) maxima (which is inferior to 1) reach 0.27 at 400 ^oC, 0.86 at 400 ^oC, 0.88 at 400 ^oC and 0.88 at 350 ^oC, respectively. In the end, using Rh/CeO_2 and Rh(N)/MgO can completely remove CO via WGS in ESR at 350 and 400 ^oC, respectively, whereas using Rh(N)/SiO_2 and Rh(N)/γ-Al_2O_3 cannot. Using Rh(N)/γ-Al_2O_3, Rh(N)/MgO and Rh(N)/CeO_2, WGS can play a major part in the production of H_2 in ESR at 400 ^oC or below, whereas using Rh(N)/SiO_2, WGS can play a minor part only. In the literature, the comparative study of Rh/Al_2O_3, Rh/MgO, Rh/SiO_2 and Rh/CeO_2 in WGS is not available yet. But it has been reported that CeO_2 is the most active support for supported Pt catalysts in WGS at 250-400 ^oC among Al_2O_3, MgO, SiO_2 and CeO_2.[83]

Table 2 Properties of transition metal oxide-supported Rh catalysts in ESR[a]

catalyst	T (°C)	C_2H_5OH conv %	H_2 yield (mol/mol C_2H_5OH)	selectivity %							$S(CO_2)/S(CO)$	$S(CO_2)//S(H_2)$
				H_2	CO_2	C_2H_4	C_2H_6	CH_4	CO	CH_3CHO		
$Rh(N)/ZrO_2$	250	53.1	1.48	46.5	0.8	0	0	27.7	41.3	30.2	0.02	0.02
	300	89.4	2.96	55.0	3.5	0.1	0.1	35.9	53.5	6.9	0.07	0.06
	350	100	4.34	72.4	57.9	0	0	34.2	7.9	0	7.3	0.80
	400	100	4.79	79.8	71.5	0	0	28.5	0	0	–	0.90
$Rh(N)/La_2O_3$	250	29.6	0.52	29.2	1.3	0	0	13.8	14.2	70.7	0.09	0.04
	300	59.2	1.55	43.5	6.2	0	0	23.5	26.4	43.9	0.23	0.14
	350	100	4.30	71.5	62.6	0	0	37.4	0	0	–	0.88
	400	100	4.77	79.5	68.9	0	0	30.2	0.7	0	96.0	0.87
$Rh(N)/Y_2O_3$	250	41.1	0.88	35.9	0.3	0	0	13.6	20.2	66.2	0.01	0.01
	300	69.1	2.04	49.0	1.9	0.6	0	21.9	36.1	39.5	0.05	0.04
	350	95.6	4.10	72.1	33.4	0	0	29.6	30.6	6.4	1.1	0.46
	400	100	4.76	79.5	67.7	0	0	28.9	3.4	0	19.8	0.85
$Rh(N)/TiO_2$	250	28.2	0.42	24.8	0.7	0.2	0	6.1	7.9	85.1	0.10	0.03
	300	41.7	0.74	29.5	1.6	0.6	0	8.2	11.1	78.5	0.14	0.05
	350	70.1	1.99	47.3	10.6	0	0	11.5	9.4	68.5	1.1	0.22
	400	93.6	3.84	68.4	33.8	0	0	28.3	22.9	15.0	1.5	0.50
Rh(N)/ZnO	250	12.4	0.15	20.0	0	0	0	5.9	6.4	87.7	0	0
	300	23.2	0.29	20.8	0	0.4	0	5.1	5.6	88.7	0.07	0
	350	57.3	1.40	40.6	8.7	0	0	10.3	10.0	71.0	0.87	0.21
	400	80.5	2.41	49.9	15.3	0	0	14.7	10.0	60.0	1.5	0.31

[a] 0.15 g of precatalyst, 1 % Rh loading in precatalysts, Ar : C_2H_5OH : H_2O = 49 : 1 : 10 molar ratio, GHSV = 26200/h, data taken 20 min later after initiation of reaction at each reaction temperature.

Transition metal oxide-supported Rh catalysts We in turn extended our catalytic screening to frequently used transition metal oxide-supported Rh catalysts ($Rh(N)/ZrO_2$, $Rh(N)/La_2O_3$, $Rh(N)/Y_2O_3$, $Rh(N)/TiO_2$ and Rh(N)/ZnO) in ESR, for the sake of demonstrating the roles of transition metal oxides in supported Rh catalysts. Table 2 shows the catalytic results of these oxide-supported Rh catalysts in ESR at 250-400 °C. $Rh(N)/ZrO_2$ performed similarly to $Rh(N)/CeO_2$ in H_2 production. Nevertheless, $Rh(N)/ZrO_2$ was less active than $Rh(N)/CeO_2$ for CH_3CHO transformation and WGS, which led to higher selectivities to CO at 350 °C and below. On the other hand, $Rh(N)/ZrO_2$ was more active than $Rh(N)/CeO_2$ for CH_4 transformation to H_2, displaying lower selectivities to CH_4 at 350 and 400 °C. The transformation of CH_4 over $Rh(N)/ZrO_2$ is assumed to proceed via MD. The weaker ability of $Rh(N)/ZrO_2$ (vs. $Rh(N)/CeO_2$) to catalyze WGS can gain support from the $S(CO_2)/S(CO)$ and $S(CO_2)/S(H_2)$ values at 350 °C and below. This outcome rendered $Rh(N)/ZrO_2$ to disable complete CO removal in ESR until 400 °C. $Rh(N)/La_2O_3$ and $Rh(N)/Y_2O_3$ exhibited low activities for H_2 production below 350 °C, because of their weak abilities in EDA, CH_3CHO transformation and WGS (as indicated by the $S(CO_2)/S(CO)$ and $S(CO_2)/S(H_2)$ values at 250 and 300 °C). However, their activities increased from 350 °C. Similar H_2 yields to those over $Rh(N)/CeO_2$ were found at 350 and 400 °C, which are consistent with their abilities to transform C_2H_5OH and CH_3CHO and catalyze WGS that increased with increasing temperature (as indicated by the $S(CO_2)/S(CO)$ values). At 350 and 400 °C, $Rh(N)/La_2O_3$ had similar activities to those of $Rh(N)/CeO_2$ for WGS and CH_4 transformation. CO was thoroughly removed at 350 °C. The transformation of CH_4 may go via MD. At 350 and 400 °C, $Rh(N)/Y_2O_3$ had a lower activity for WGS than $Rh(N)/CeO_2$ and a higher activity for CH_4 transformation than $Rh(N)/CeO_2$. The transformation of

CH_4 may proceed via MD and steam reforming of adsorbed CH_x (x = 1-3). Rh(N)/TiO_2 and Rh(N)/ZnO apparently showed rather low activities for H_2 production in the whole temperature range, due to their rather weak abilities in EDA, CH_3CHO transformation and WGS (as indicated by the S(CO_2)/S(CO) and S(CO_2)/S(H_2) values). They gave rise to only 3.84 and 2.41 mol H_2/mol C_2H_5OH at 400 ^oC, respectively. At the same time that higher selectivities to CO were observed, lower selectivities to CH_4 were achieved owing to a higher activity for MSR. During the ESR process over Rh(N)/ZnO, $(CH_3)_2CO$ was not observed, possibly due to the use of a GHSV as high as 26200/h. It is documented that $(CH_3)_2CO$ can be produced during ESR over ZnO and that the selectivity to $(CH_3)_2CO$ drops remarkably with increasing GHSV.[21]

Based on the catalytic results in Tables 1 and 2, the following can be summarized on the frequently used oxide-supported Rh catalysts for low-temperature ESR.

(1) Rh(N)/CeO_2, Rh(N)/ZrO_2 and Rh(N)/γ-Al_2O_3 are generally advantageous in H_2 production, followed by Rh(N)/La_2O_3 and Rh(N)/Y_2O_3.

(2) typical oxide-supported Rh catalysts in Table 1 are more active than the transition metal oxide-supported ones in Table 2 in CH_3CHO transformation including AD and ASR.

(3) Rh(N)/CeO_2 is advantageous in WGS, followed by Rh(N)/La_2O_3 and Rh(N)/ZrO_2.

(4) All these catalysts are disadvantageous in ASR and CH_4 transformation. Rh(N)/ZnO, Rh(N)/TiO_2, Rh(N)/Y_2O_3 and Rh(N)/ZrO_2 are slightly more active for CH_4 transformation, followed by Rh(N)/La_2O_3 and Rh(N)/CeO_2.

Various Rh precursor-derived CeO_2-supported Rh catalysts As observed above, CeO_2 behaves as an advantageous support over the other oxides to produce an effective supported Rh catalyst for H_2 generation from ESR. We next studied the effect of Rh precursor on the catalytic behaviour of a CeO_2-supported Rh catalyst in ESR. Table 3 compares the catalytic results of CeO_2-supported Rh catalysts derived from $Rh(NO_3)_3 \cdot xH_2O$, $RhCl_3 \cdot xH_2O$, $Rh(acac)_3$ and $Rh_4(CO)_{12}$ in ESR at 250-400 ^oC. Similar to Rh(N)/CeO_2, Rh(A)/CeO_2 and Rh(C)/CeO_2 had good catalytic performances, producing higher H_2 yields in the whole temperature range. Both of them were quite active for WGS in terms of S(CO_2)/S(CO) and S(CO_2)/S(H_2). Above all, CO could be fully removed at 350 and 400 ^oC over Rh(C)/CeO_2. In contrast to these three catalysts, Rh(Cl)/CeO_2 led to lower C_2H_5OH conversions, concomitant with lower H_2 yields below 400 ^oC. The results are evidently attributed to a lower activity of Rh(Cl)/CeO_2 for CH_3CHO transformation and WGS, as seen in the selectivities to CH_3CHO and CO, the S(CO_2)/S(CO) and S(CO_2)/S(H_2) values. The activity lowering is caused probably by the modification of the Rh/CeO_2 surface properties in the presence of Cl.[84-86] It is known that in a

Table 3 Properties of various Rh precursor-derived CeO_2-supported Rh catalysts in ESR[a]

catalyst	T (°C)	C_2H_5OH conv. %	H_2 yield (mol/mol C_2H_5OH)	selectivity %							S(CO_2)/S(CO)	S(CO_2)//S(H_2)
				H_2	CO_2	C_2H_4	C_2H_6	CH_4	CO	CH_3CHO		
Rh(N)/CeO_2	250	40.9	1.35	55.2	5.6	0	0	32.9	45.5	16.0	0.12	0.10
	300	94.1	3.60	63.8	19.1	0	0.2	36.3	42.7	1.7	0.45	0.30
	350	100	4.18	69.7	61.2	0	0	38.8	0	0	–	0.88
	400	100	4.70	78.4	68.4	0	0	30.1	1.5	0	42.6	0.87
Rh(Cl)/CeO_2	250	23.6	0.61	42.7	0	0	0	24.0	34.2	41.8	0	0
	300	48.9	1.63	55.5	1.4	0	0	29.4	49.3	19.9	0.03	0.03
	350	85.9	3.55	68.9	12.7	0	0	29.1	52.5	5.7	0.21	0.18
	400	100	4.66	77.6	53.5	0	0	29.1	17.2	0.2	3.1	0.69
Rh(A)/CeO_2	250	43.4	1.42	54.8	5.0	0	0	36.4	46.1	17.5	0.11	0.09
	300	81.8	2.98	60.5	19.6	0	0.3	37.2	37.4	5.5	0.52	0.32
	350	100	4.27	71.2	60.3	0	0	37.3	2.4	0	25.1	0.85
	400	100	4.12	68.9	59.5	0	0	40.0	0.5	0	117	0.80
Rh(C)/CeO_2	250	59.4	1.82	51.0	2.1	0	0	35.5	48.6	13.8	0.04	0.04
	300	99.9	3.74	62.4	10.8	0	0.6	36.3	52.3	0	0.21	0.17
	350	100	4.18	69.7	61.4	0	0	38.5	0	0	–	0.88
	400	100	4.73	78.8	70.4	0	0	29.6	0	0	–	0.89

[a] 0.15 g of precatalyst, 1 % Rh loading in precatalysts, Ar : C_2H_5OH : H_2O = 49 : 1 : 10 molar ratio, GHSV = 26200/h, data taken 20 min later after initiation of reaction at each reaction temperature, excluding trace $(CH_3)_2CO$ at 250 and 300 °C.

Table 4 Properties of CeO_2-supported Rh catalysts with different Rh loadings in ESR[a]

Rh loading (%)	T (°C)	C_2H_5OH conv. %	H_2 yield (mol/mol C_2H_5OH)	selectivity %								S(CO_2)/S(CO)	S(CO_2)//S(H_2)
				H_2	CO_2	C_2H_4	C_2H_6	CH_4	CO	CH_3CHO	$(CH_3)_2CO$		
0.1	250	30.2	0.74	40.5	4.0	0	0	25.5	26.3	42.4	1.8	0.15	0.10
	300	46.4	1.26	44.6	8.3	0	0	19.3	20.3	41.6	10.5	0.41	0.19
	350	83.2	2.88	57.7	17.7	0	0	18.8	21.0	18.3	24.2	0.84	0.31
	400	100	4.76	79.4	68.2	0	0	28.7	3.1	0	0	22.0	0.86
0.3	250	31.1	0.81	44.6	3.0	0	0	27.3	33.2	36.2	0.3	0.09	0.07
	300	64.5	1.96	50.7	6.5	0	0	34.0	40.9	16.8	1.8	0.16	0.13
	350	99.9	4.03	67.3	44.0	0	0	38.2	16.4	0.5	0	2.68	0.65
	400	100	4.52	75.4	64.1	0	0	33.5	2.4	0	0	26.7	0.85
1.0	250	40.6	1.33	54.6	5.4	0	0	32.3	45.7	16.3	0.7	0.12	0.10
	300	94.0	3.56	63.2	17.6	0	0.2	35.9	43.2	1.7	1.4	0.41	0.28
	350	100	4.17	69.7	61.2	0	0	38.8	0	0	0	–	0.88
	400	100	4.70	78.4	68.4	0	0	30.1	1.5	0	0	42.6	0.87
2.8	250	46.4	1.58	56.7	2.9	0	0	31.7	51.4	14.0	0	0.06	0.05
	300	94.7	3.63	63.9	9.4	0	0	34.0	54.8	1.5	0.3	0.17	0.15
	350	100	4.14	69.1	59.3	0	0	40.7	0	0	0	–	0.86
	400	100	4.71	78.5	68.1	0	0	30.3	1.6	0	0	42.6	0.87

[a] 0.15 g of Rh^{3+}(N)/CeO_2, Ar : C_2H_5OH : H_2O = 49 : 1 : 10 molar ratio, GHSV = 26200/h, data taken 20 min later after initiation of reaction at each reaction temperature.

Rh(Cl)/CeO_2 sample, all of the Cl can be retained on the CeO_2 lattice via substitution with the lattice O after thermal treatment in H_2 even at 900 °C.[84,87] The presence of Cl in the CeO_2 lattice can alter the redox behaviour of CeO_2 and influence the surface chemistry of Rh/CeO_2.[85,86] As a result, the catalytic activity of Rh/CeO_2 for ESR can be influenced. Meanwhile, it was noticed that none of the four catalysts was active enough for ASR to convert more CH_4 to H_2 at 400 °C and below in terms of the selectivity to CH_4.

Nonetheless, Rh(N)/CeO_2, Rh(A)/CeO_2 and Rh(C)/CeO_2 apparently perform better than Rh(Cl)/CeO_2 for H_2 generation from ESR.

CeO_2-supported Rh catalysts with different Rh loadings To reveal the effect of dispersion of Rh metal on CeO_2 on H_2 generation from ESR, we examined the catalytic properties of CeO_2-supported Rh catalysts with different Rh loadings in ESR. Table 4 gives the catalytic results of CeO_2-supported

Table 5 Properties of CeO_2-supported Rh catalysts from calcined precatalysts in ESR[a]

calcination T (°C)	reaction T (°C)	C_2H_5OH conv. %	H_2 yield (mol/mol C_2H_5OH)	selectivity %							$S(CO_2)/S(CO)$	$S(CO_2)//S(H_2)$
				H_2	CO_2	C_2H_4	C_2H_6	CH_4	CO	CH_3CHO		
21	250	40.9	1.35	55.2	5.6	0	0	32.9	45.5	16.0	0.12	0.10
	300	94.1	3.60	63.8	19.1	0	0.2	36.3	42.7	1.7	0.45	0.30
	350	100	4.18	69.7	61.2	0	0	38.8	0	0	–	0.88
	400	100	4.70	78.4	68.4	0	0	30.1	1.5	0	42.6	0.87
400	250	27.0	0.91	56.0	1.6	0	0	29.2	53.2	16.0	0.03	0.03
	300	68.7	2.53	61.3	5.6	0	0	31.5	59.0	3.9	0.10	0.09
	350	99.1	4.17	70.1	49.8	0	0	31.6	18.0	0.6	2.8	0.71
	400	100	4.66	77.6	70.7	0	0	27.0	2.3	0	30.6	0.91
700	250	21.9	0.67	50.6	4.4	0	0	19.4	36.7	39.5	0.12	0.09
	300	47.2	1.81	63.9	19.2	0	0.3	22.6	38.9	19.0	0.49	0.30
	350	98.4	4.49	76.1	59.2	0	0	26.6	12.3	1.9	4.8	0.78
	400	100	4.82	80.2	73.3	0	0	24.5	2.2	0	33.9	0.91

[a] 0.15 g of calcined $Rh^{3+}(N)/CeO_2$, 1 % Rh loading in $Rh^{3+}(N)/CeO_2$, Ar : C_2H_5OH : H_2O = 49 : 1 : 10 molar ratio, GHSV = 26200/h, data taken 20 min later after initiation of reaction at each reaction temperature, excluding trace $(CH_3)_2CO$ at 250-350 °C.

Rh catalysts prepared from $Rh(NO_3)_3 \cdot xH_2O$ with Rh loadings varying from 0.1 to 2.8 % in ESR at 250-400 °C. Below 350 °C, the C_2H_5OH conversion, CH_3CHO transformation, $(CH_3)_2CO$ transformation and H_2 yield increased with increasing Rh loading. This relationship is in line with the fact that the supported Rh can promote all the reaction pathways on CeO_2. However, it looks as if the specific catalytic activity of $Rh(N)/CeO_2$ decreases markedly with increasing Rh loading. This suggests that the dispersion of Rh metal on CeO_2 declines with increasing Rh loading. Although a lower Rh loading led to more efficient H_2 production, it disabled complete removal of CO at 400 °C and below. From the $S(CO_2)/S(CO)$ values, a lower Rh loading leads to a higher catalytic activity of $Rh(N)/CeO_2$ for WGS at 250 °C. But its catalytic activity for WGS rises slowly with increasing reaction temperature, differing from that with a higher Rh loading which rises more rapidly with increasing reaction temperature. The variation of $S(CO_2)/S(H_2)$ with Rh loading indicates that the higher the Rh loading on CeO_2, the more the contribution of WGS to the total production of H_2 increases with increasing reaction temperature at 250-350 °C. Meanwhile, a very low Rh loading (0.1 %) led to a slight decrease in the selectivity to CH_4 and thus a slight increase in the selectivity to H_2 at 400 °C , which suggests that the high Rh dispersion on CeO_2 favours accelerating MD and steam reforming of adsorbed CH_x (x = 1-3). It was noticed that the selectivity to $(CH_3)_2CO$ over $Rh(N)/CeO_2$ decreased with increasing Rh loading, which further suggests that $(CH_3)_2CO$ transformation dominates over EDAC by competition in the presence of Rh. The 1.0 % Rh loading on CeO_2 appears more favourable for ESR in terms of H_2 production, CH_4 transformation and CO removal. Rh loadings above 1 % seem helpless for improving the catalytic performance of $Rh(N)/CeO_2$ in ESR.

CeO_2-supported Rh catalysts from calcined precatalysts To demonstrate the effect of strong metal-support interaction on H_2 generation from ESR, we looked into the catalytic properties of CeO_2-supported Rh catalysts from calcined precatalysts in ESR. Table 5 presents the catalytic results of CeO_2-supported Rh catalysts from $Rh^{3+}(N)/CeO_2$ calcined at different temperatures in ESR at 250-400 °C. At 250 and 300 °C, $Rh^{3+}(N)/CeO_2$ calcined at 400 and 700 °C led to significant decreases in the

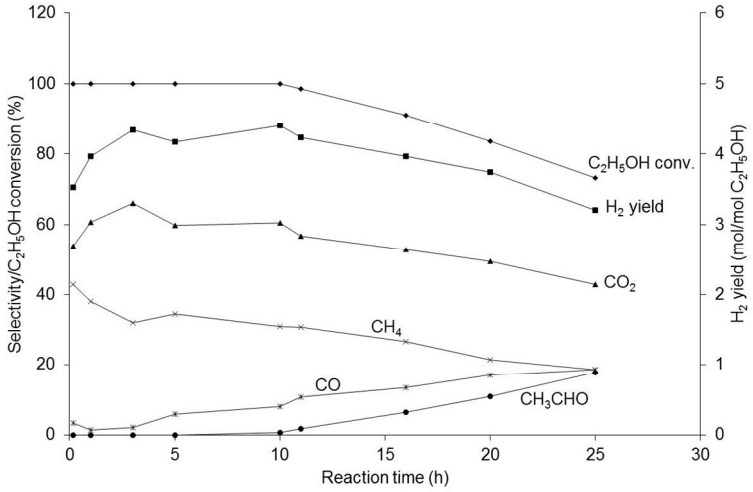

Fig. 5 On stream ESR profiles over Rh(N)/CeO_2 at 350 ^oC.

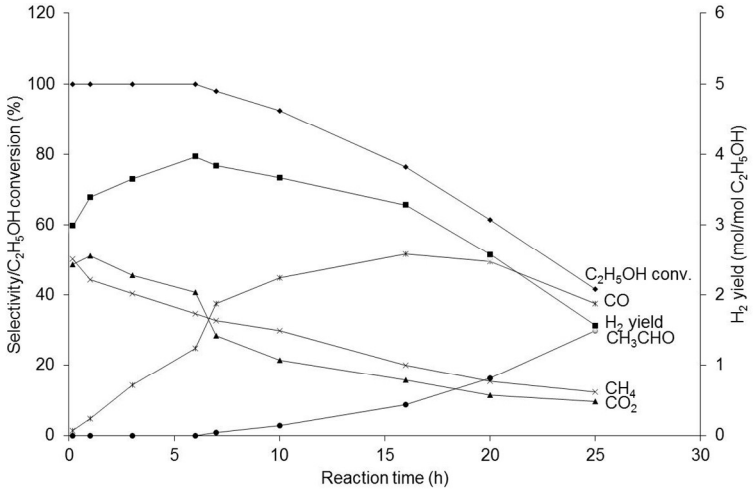

Fig. 6 On stream ESR profiles over Rh(A)/CeO_2 at 350 ^oC.

C_2H_5OH conversion, CH_3CHO transformation and H_2 production. The C_2H_5OH conversion, CH_3CHO transformation and H_2 yield decreased obviously with increasing calcination temperature. Trace $(CH_3)_2CO$ was detected only at 250 and 300 ^oC. In the whole temperature range, calcined Rh^{3+}(N)/CeO_2 gave rise to a finitely decreased selectivity to CH_4 with increasing calcination temperature. Meanwhile, Rh^{3+}(N)/CeO_2 calcined at 400 and 700 ^oC led to an increased selectivity to CO so that CO could not be thoroughly eliminated in ESR, consistent with the S(CO_2)/S(CO) values. Accordingly, calcination of Rh^{3+}(N)/CeO_2 is helpless for improving the catalytic performance of Rh(N)/CeO_2 in H_2 generation from ESR. Comparing Tables 4 and 5, it is noted that the catalytic behaviour of Rh(N)/CeO_2 with increasing calcination temperature is similar to that of Rh(N)/CeO_2 with decreasing Rh loading, which hints that the dispersion of Rh metal on CeO_2 may increase with increasing calcination

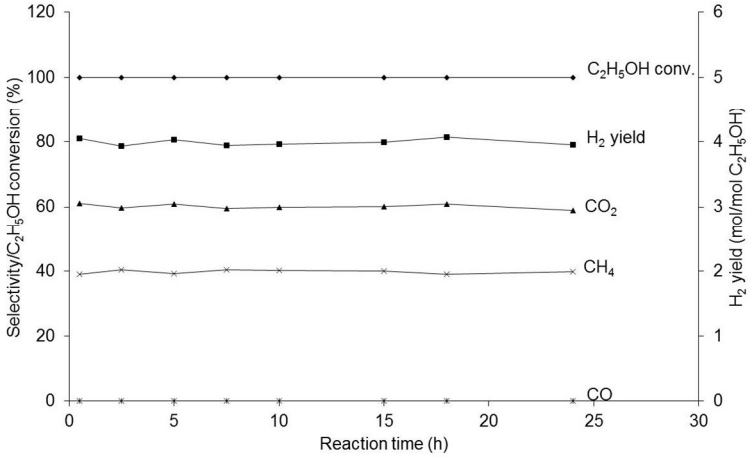

Fig. 7 On stream ESR profiles over Rh(C)/CeO_2 at 350 °C.

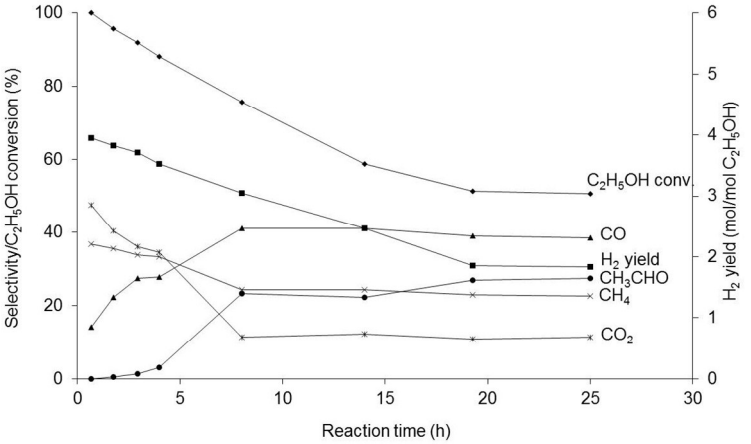

Fig. 8 On stream ESR profiles over Rh(C)/CeO_2 at 300 °C.

temperature.

Catalytic stability of CeO_2-supported Rh catalysts Since Rh/CeO_2 turned out to be more effective than the other oxide-supported Rh catalysts in H_2 generation from low-temperature ESR, we finally paid our attention to the catalytic stability of Rh/CeO_2 in low-temperature ESR. Figs. 5-7 illustrate the on stream reaction profiles over three typical Rh precursor-derived CeO_2-supported Rh catalysts at 350 °C. Rh(N)/CeO_2 deactivated gradually with reaction time (Fig. 5). The C_2H_5OH conversion and H_2 yield did not deplete within the initial 10 h but dropped to 73.2 % and 3.20 mol/mol C_2H_5OH at 25 h. During 25 h of reaction, the selectivities to CO and CH_3CHO increased to 18.5 and 17.6 % from 3.4 and 0 %, respectively, while the selectivity to CH_4 decreased to 18.5 % from 42.8 %. The drop in the H_2 yield coincided well with the decrease in the selectivity to CO_2 and the increase in the selectivity to CO, accounting for the deterioration of catalytic activity for WGS. Meanwhile, the increase in the selectivity

Table 6 Thermodynamic[a] and catalytic[b] data of ESR

	T (°C)	C_2H_5OH conv. %	H_2 yield (mol/mol C_2H_5OH)	selectivity % H_2	CO	CO_2	CH_4	$S(CO_2)/S(CO)$	$S(CO_2)//S(H_2)$
thermodynamic	300	100	2.4	34	1	33	66	33	0.97
equilibrium	400	100	4.2	70	4	51	45	13	0.73
	500	100	5.5	92	9	72	19	8.0	0.78
$Rh(N)/CeO_2$	300	94.1	3.60	63.8	42.7	19.1	36.3	0.45	0.30
	400	100	4.70	78.4	1.5	68.4	30.1	42.6	0.87
	500	100	5.86	97.7	9.8	86.3	3.8	8.7	0.88
$Rh(C)/CeO_2$	300	99.9	3.74	62.4	52.3	10.8	36.3	0.21	0.17
	400	100	4.73	78.8	0	70.4	29.6	–	0.89
	500	100	5.82	97.0	6.9	88.0	5.0	12.4	0.91

[a] From Ref. 90, Ar : C_2H_5OH : H_2O = 49 : 1 : 9 molar ratio, $Y(H_2) = X(C_2H_5OH) \times S(H_2) \times 6$. [b] 0.15 g of precatalyst, 1 % Rh loading in precatalysts, Ar : C_2H_5OH : H_2O = 49 : 1 : 10 molar ratio, GHSV = 26200/h, data taken 20 min later after initiation of reaction at each reaction temperature.

to CH_3CHO was accompanied by the decrease in the selectivity to CH_4, indicating the catalyst deactivation for AD. $Rh(A)/CeO_2$ deactivated more rapidly than $Rh(N)/CeO_2$ with reaction time (Fig. 6). The C_2H_5OH conversion and H_2 yield started to decline after 6 h, and dropped to 41.5 % and 1.56 mol/mol C_2H_5OH at 25 h. At 25 h, the selectivities to CO, CH_4 and CH_3CHO were observed at 37.5, 12.2 and 29.8 %, respectively. In contract, $Rh(C)/CeO_2$ displayed stable catalytic performance during at least 24 h of reaction (Fig. 7). At 24 h, a C_2H_5OH conversion of 100 % and an H_2 yield of 3.96 mol/mol C_2H_5OH were obtained with the concomitant production of CH_4 (39.7 % S) and no CO. During the 24 h reaction, all the catalytic properties including C_2H_5OH conversion and selectivities to all the products remained substantially unchanged, which significantly showed a good catalytic stability of $Rh(C)/CeO_2$. Nevertheless, no satisfactory catalytic stability could be achieved at 300 °C, as shown in Fig. 8. The catalyst deactivated rapidly. The C_2H_5OH conversion and H_2 yield dropped from 100 to 51.3 % and from 3.95 to 1.85 mol/mol C_2H_5OH within 19 h.

Kinetic control It is of significance to stress kinetic control under thermodynamically favourable conditions for the purpose of achieving a high H_2 yield against undesirable products in low-temperature ESR. Several studies by different authors[4,8,14] have reported that in the presence of their supported metal catalysts at 450-800 °C, the selectivity values to H_2 are significantly higher than the thermodynamic equilibrium values.[4,8-13] In low-temperature ESR, the different yields of H_2 and selectivities to products can be obtained over the various oxides and various oxide-supported Rh catalysts, as indicated in our catalytic results. Although these catalysts accelerate all the related reaction pathways during ESR as a whole, the extents to which the reaction pathways are accelerated are different. The CeO_2-supported highly dispersed Rh catalysts favour enhancing the H_2 yield and reducing the selectivity to CH_4, however they unfavour reducing the selectivity to CO. $Rh(C)/CeO_2$ with a 1 % Rh loading acts as an appropriate catalyst to lead to complete removal of CO although it is less active for CH_4 transformation. In the complex ESR process consisting of multiple reaction pathways, the roles of catalysts should be to not just

speed up the formation of H_2 but also kinetically limit the formation of undesired products. Desired reaction pathways should be accelerated whereas undesired reaction pathways should be depressed. We expect a successful catalyst design to kinetically control the relative rates of reaction pathways during low-temperature ESR and thus reach a desired product distribution.

Now let us make a comparison between the catalytic performance of our typical Rh/CeO_2 catalysts and the thermodynamic analysis for low-temperature ESR. Like in almost all the reported catalytic studies of ESR, we adopted dilution of the reaction feed with an inert gas as carrier gas in our ESR reaction at atmospheric pressure. Although addition of inert gas has a positive effect on the equiibrium H_2 yield at low temperatures,[14,88-90] only a more complete study on the thermodynamic analysis of ESR with diluted systems has been reported by Hernández and Kafarov to date.[90] This thermodynamic analysis of ESR applied comparable conditions to those used in our ESR experiments. Hence, it can provide some useful information for our reference. As shown in Table 6, the thermodynamic calculations in equlibrium conditions predict that the C_2H_5OH conversion is complete and that the H_2 yield increases with increasing reaction temperature at 300-500 ^oC. At the same time, the selectivity to CO increases with increasing reaction temperature while the selectivity to CH_4 decreases with increasing reaction temperature. The prominent increase in $S(CO_2)/S(CO)$ with decreasing reaction temperature implies that low temperatures favour WGS in thermodynamics. When using our $Rh(N)/CeO_2$ or $Rh(C)/CeO_2$ as a catalyst, the H_2 yields exceed the thermodynamic equilibrium values at 300-500 ^oC. The value differences increase as the reaction temperature decreases and become salient at 300 ^oC. This accounts for that H_2 generation from ESR is strongly controlled by kinetics in the presence of either $Rh(N)/CeO_2$ or $Rh(C)/CeO_2$ at low temperatures. But as reaction temperature increases, the H_2 yields gradually approach the thermodynamic equilibrium values, which indicates that H_2 generation from ESR tends to lose kinetic control at high temperatures. On the other hand, the selectivity to CO is much higher than the thermodynamic equilibrium value and thereby the $S(CO_2)/S(CO)$ value is much lower than the thermodynamic equilibrium value at 300 ^oC. The comparative selectivity to CO and $S(CO_2)/S(CO)$ values are contrary at 400 ^oC. Meanwhile the selectivity to CH_4 is remarkably inferior to the thermodynamic equilibrium value from 300 to 500 ^oC. Out of the thermodynamic predictions, our catalytic results suggest that $Rh(N)/CeO_2$ and $Rh(C)/CeO_2$ promote H_2 generation from ESR via ASR, ACSR and WGS at 300 ^oC, and via ASR, ACSR, MD, steam reforming of adsorbed CH_x (x = 1-3) and WGS at 400 ^oC, which are also reflected in the different $S(CO_2)/S(H_2)$ values.

Surface Properties of Catalysts

TPR pertinent to Rh precatalysts Fig. 9 shows the TPR patterns of various oxide-supported $Rh(NO_3)_3$

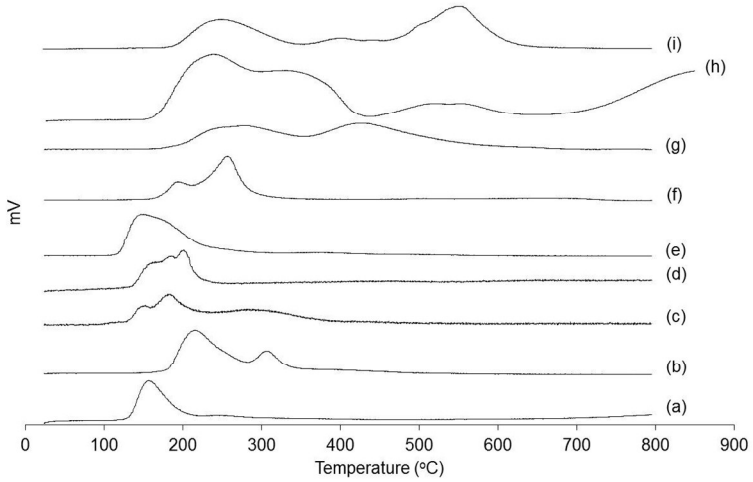

Fig. 9 TPR profiles of (a) $Rh^{3+}(N)/CeO_2$; (b) $Rh^{3+}(N)/SiO_2$; (c) $Rh^{3+}(N)/Al_2O_3$; (d) $Rh^{3+}(N)/ZrO_2$; (e) $Rh^{3+}(N)/TiO_2$; (f) $Rh^{3+}(N)/ZnO$; (g) $Rh^{3+}(N)/Y_2O_3$; (h) $Rh^{3+}(N)/La_2O_3$ and (i) $Rh^{3+}(N)/MgO$.

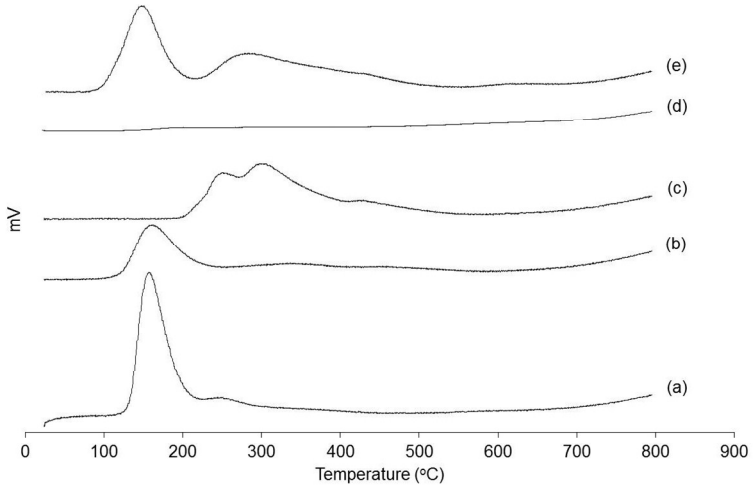

Fig. 10 TPR profiles of (a) $Rh^{3+}(N)/CeO_2$, (b) $Rh^{3+}(Cl)/CeO_2$, (c) $Rh^{3+}(A)/CeO_2$, (d) $Rh_4(C)/CeO_2$ pretreated in air at 21 °C and (e) $Rh_4(C)/CeO_2$ pretreated in air at 110 °C.

precatalysts following 2 h of drying in vacuum (10^{-2} torr) at 21 °C. Under equivalent conditions, there was no H_2 consumption below 450 °C in the TPR processes of all the supports used alone. After 2 h of drying in vacuum at 21 °C, all the $Rh^{3+}(N)$/oxide samples remained unchanged in colour. Moreover the amounts of H_2 consumed in the TPR processes of all the $Rh^{3+}(N)$/oxide samples highly exceeded the stoichiometric value for the complete reduction of Rh^{3+}. It is thus assumed that $Rh(NO_3)_3$ on these supports would not decompose after drying at 21 °C and that the surplus H_2 consumption would be due to the reduction of NO_3^- (plus Ce^{4+} for $Rh^{3+}(N)/CeO_2$). As expected, the number and temperature of TPR peaks of such $Rh^{3+}(N)$/oxide depended on the nature of the interaction of $Rh(NO_3)_3$ with the support surface. The TPR pattern of $Rh^{3+}(N)/CeO_2$ exhibited an intense peak at 160 °C, a weak one around 252 °C and a very weak one around 380 °C. The first peak may be assigned to the reduction of NO_3^- [40,91] and

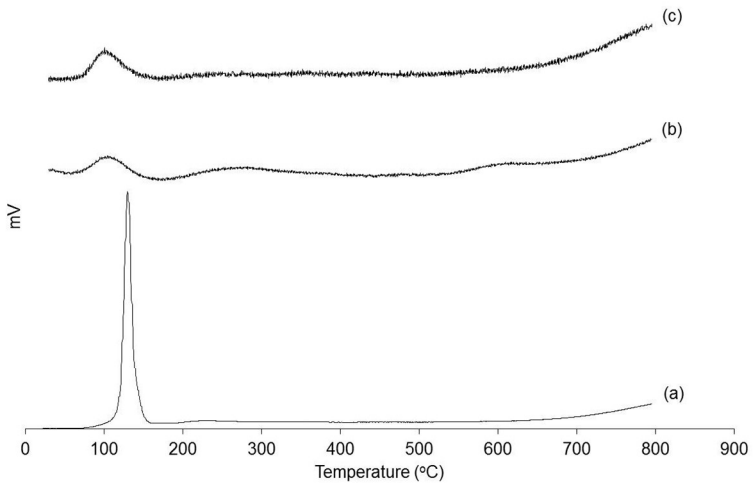

Fig. 11 TPR profiles of $Rh^{3+}(N)/CeO_2$ calcined at (a) 110 °C, (b) 400 °C and (c) 700 °C.

Rh^{3+} which is in weak interaction with CeO_2, the second one may be attributed to the reduction of Rh^{3+} in bulk-like $Rh(NO_3)_3$, while the last one may be a result of the shoulder peak shift to lower temperatures for the reduction of surface Ce^{4+} and carbonates because of H spillover from Rh to the support.[92] Since the CeO_2 used here has a very low surface area and moreover the Rh^{3+}-CeO_2 interaction is very weak, the observed H spillover effect is negligible (see ESI). On $Rh^{3+}(N)/SiO_2$, $Rh^{3+}(N)/\gamma$-Al_2O_3, $Rh^{3+}(N)/ZrO_2$, $Rh^{3+}(N)/TiO_2$ and $Rh^{3+}(N)/ZnO$, similarly, the TPR patterns gave a peak or two overlapping peaks at lower temperatures due to the reduction of NO_3^- and Rh^{3+} in weak interaction with the supports, and a peak at higher temperatures due to the reduction of Rh^{3+} in bulk-like $Rh(NO_3)_3$. On $Rh^{3+}(N)/Y_2O_3$, $Rh^{3+}(N)/La_2O_3$ and $Rh^{3+}(N)/MgO$, in contrast, one or two extra peaks appeared at 427-560 °C apart from the above mentioned normal ones due to supported $Rh(NO_3)_3$. These extra peaks may be related to the strong Rh^{3+}-support interaction, as described in the literature.[93] For $Rh^{3+}(N)$/oxide, the relative strength of the interaction between Rh^{3+} and support can be roughly evaluated by the relative Rh^{3+} reduction peak shift to higher temperatures. In virtue of the TPR results in Fig. 9, the order of the strength of Rh^{3+}-support interaction can be ranked as $Rh^{3+}(N)/MgO > Rh^{3+}(N)/La_2O_3 > Rh^{3+}(N)/Y_2O_3 > Rh^{3+}(N)/SiO_2 > Rh^{3+}(N)/ZnO > Rh^{3+}(N)/\gamma$-$Al_2O_3 > Rh^{3+}(N)/ZrO_2 > Rh^{3+}(N)/TiO_2 > Rh^{3+}(N)/CeO_2$. As these $Rh^{3+}(N)$/oxide samples are not subjected to any treatments prior to TPR, the strong Rh^{3+}-support interaction observed in $Rh^{3+}(N)/Y_2O_3$, $Rh^{3+}(N)/La_2O_3$ and $Rh^{3+}(N)/MgO$ may be caused by heating during the TPR experiments, which may produce surface Rh oxides before reduction at higher temperatures. It is noteworthy that except the fractions of surface Rh oxides in $Rh^{3+}(N)/Y_2O_3$, $Rh^{3+}(N)/La_2O_3$ and $Rh^{3+}(N)/MgO$, all of the $Rh(NO_3)_3$ normally supported on the oxides seems to be fully reduced at 400 °C.

From the above TPR results, $Rh^{3+}(N)/CeO_2$ has weaker Rh^{3+}-support interaction than the other

Rh^{3+}(N)/oxide precatalysts studied. To reveal the effect of Rh precursor on the Rh^{3+}-support interaction, we next conducted further TPR experiments with Rh^{3+}(Cl)/CeO_2, Rh^{3+}(A)/CeO_2 pretreated in vacuum at 21 ^oC, and Rh_4(C)/CeO_2 pretreated in air at 21 and 110 ^oC (see ESI). As shown in Fig. 10, the presence of Rh influenced little the reduction peaks of Ce^{4+} so that the H spillover effect from Rh to CeO_2 could be neglected. For Rh^{3+}(Cl)/CeO_2, an intense peak at 158 ^oC and two weak ones around 335 and 461 ^oC were observed, which may be ascribed to the reduction of Rh^{3+} in weak interaction with CeO_2, bulk-like $RhCl_3$ and a surface Rh oxide formed via the strong Rh^{3+}-CeO_2 interaction, respectively. For Rh^{3+}(A)/CeO_2, two broad, intense peaks at 251 and 300 ^oC appeared together with a shoulder one near 431 ^oC. It is known that oxide-supported transition metal acetylacetonates are stable at room temperature[94] and that decomposition of $Rh(acac)_3$ is complete at 267 ^oC under Ar[95] and acac groups are fully away from $Rh(acac)_3$/TiO_2 at 250 ^oC under vacuum .[96] Thus, the two peaks at 251 and 300 ^oC may correspond to the reduction of Rh^{3+} in weak interaction with CeO_2 and Rh^{3+} in bulk-like $Rh(acac)_3$, respectively. The reduction of acac groups in Rh^{3+}(A)/CeO_2, if possible, may occur near 251 ^oC. The peak at 431 ^oC may be due to the reduction of a surface Rh oxide formed via the strong Rh^{3+}-CeO_2 interaction. As for Rh_4(C)/CeO_2, the TPR pattern after 5 h of exposure to air at 21 ^oC showed only a couple of tiny signals, which implies that the Rh^0 in Rh_4(C)/CeO_2 is oxidized in air at 21 ^oC negligibly. After treatment in air at 110 ^oC, the TPR pattern exhibited a strong peak at 148 ^oC, a medium one at 285 ^oC and a shoulder one near 440 ^oC. These three peaks can be attributed to the reduction of Rh^{3+} in weak interaction with CeO_2, a bulk-like Rh oxide and a surface Rh oxide formed via the strong Rh^{3+}-CeO_2 interaction, respectively. It is deemed that the reduction of CO groups in Rh_4(C)/CeO_2 pretreated in air does not take place during TPR, in that oxide-supported Rh carbonyls seem to fully decarbonylate below 200 ^oC.[97] From Fig. 10, the TRP profiles of Rh^{3+}(Cl)/CeO_2, Rh^{3+}(A)/CeO_2 and oxidized Rh_4(C)/CeO_2 displayed a weak peak at 432-465 ^oC possibly due to the reduction of a surface Rh oxide in small amounts formed via the strong Rh^{3+}-CeO_2 interaction. This was not the case for Rh^{3+}(N)/CeO_2 and slightly oxidized Rh_4(C)/CeO_2. Except these small amounts of the surface Rh oxide, all of the Rh^{3+} normally supported on CeO_2 seems to be fully reduced at 400 ^oC.

We finally checked the influence of calcination on the Rh^{3+}-CeO_2 interaction by TPR, since calcination of oxide-supported metal precatalysts plays an important role in determining catalytic performance of oxide-supported metal catalysts. TPR experiments of Rh^{3+}(N)/CeO_2 after calcination in air were conducted. Fig. 11 shows the TPR patterns of Rh^{3+}(N)/CeO_2 calcined at different temperatures. The calcination pretreatments did not seem to alter the reductive behaviour of Ce^{4+} and reinforce the H spillover effect from Rh to CeO_2. The calcination at 110 ^oC enabled decomposition of the supported $Rh(NO_3)_3$ to give the supported Rh_2O_3 with the evolution of NO_2.[39] The resulting

Rh_2O_3/CeO_2 had a sharp peak at 129 ^oC due to the reduction of Rh^{3+} in weak interaction with CeO_2, and a very weak one at 218 ^oC due to the reduction of trace amounts of bulk-like Rh_2O_3. However, the calcination at 400 ^oC led to a downward shift of the first peak from 129 to 108 ^oC and the appearance of a new, broad one centred at 285 ^oC. The downward shift appears to account for the formation of smaller Rh particles via smaller Rh_2O_3 particles formed via strenthened Rh^{3+}-CeO_2 interaction at 400 ^oC. The appearance of the broad peak at 285 ^oC may implicate the emergence of stronger Rh^{3+}-CeO_2 interaction for Rh^{3+} at the interface. When the calcination temperature was raised to 700 ^oC, the first peak continued to shift downward to 102 ^oC and the peak at 285 ^oC dropped in intensity. The results may be attributed to further strenthened Rh^{3+}-CeO_2 interaction upon calcination at 700 ^oC resulting in even smaller Rh_2O_3 particles on the one hand, and to heavy sintering of CeO_2 leading to a reduced surface area of CeO_2 and thus decreased amounts of a surface Rh oxide on the other hand.[98] It is known that the surface area of CeO_2 is almost unaffected by calcination below 400 ^oC, but decreases obviously with increasing calcination temperature above 400 ^oC.[98] These TPR results suggest that higher calcination temperatures strengthen the Rh^{3+}-CeO_2 interaction in $Rh^{3+}(N)/CeO_2$, which may lead to the formation of smaller supported Rh particles, coinciding with the catalytic behaviour of $Rh(N)/CeO_2$ in ESR with increasing calcination temperature (Table 5). However, it is difficult to estimate the variation of the amounts of surface Rh_2O_3 and an irreducible surface Rh oxide on CeO_2 caused by the stronger Rh^{3+}-CeO_2 interaction from the TPR results. It is unclear why the calcination at 700 ^oC results in an increased intensity in the reduction peak of surface Rh_2O_3 on CeO_2, as compared with the case of the calcination at 400 ^oC.

Overall, the TPR processes pertinent to the various oxide-supported Rh precatalysts studied produce supported Rh particles from supported Rh^{3+} in weak interaction with the supports, supported bulk-like Rh compounds and surface Rh oxides, depending on the strength of the interaction of Rh precursors with oxides. $Rh^{3+}(N)/CeO_2$ has weaker Rh^{3+}-support interaction than the other oxide-supported Rh precatalysts, so that its TPR process gives rise to supported Rh particles only from supported Rh^{3+} in weak interaction with CeO_2 and supported bulk-like $Rh(NO_3)_3$. $Rh^{3+}(N)/MgO$, $Rh^{3+}(N)/La_2O_3$ and $Rh^{3+}(N)/Y_2O_3$ possess strong Rh^{3+}-support interaction, so that their TPR processes yield supported Rh particles from surface Rh oxides besides supported bulk-like Rh compounds. Use of $RhCl_3 \cdot xH_2O$ and $Rh(acac)_3$ as precursors slightly promotes the strong Rh^{3+}-CeO_2 interaction which results in the formation of small amounts of supported surface Rh oxides. Use of $Rh_4(CO)_{12}$ as a precursor avoids the strong Rh^{3+}-CeO_2 interaction and thus the formation of a surface Rh oxide. With high-temperature calcination pretreatments, the Rh^{3+}-support interaction in Rh^{3+}/oxide gets efficiently

Table 7 H_2 chemisorption measurements of fresh CeO_2-supported Rh catalysts[a]

Catalyst	Rh loading %	chemisorbed H_2 (μmol/g)	apparent H/Rh (atomic ratio)
–	0	0	–
Rh(N)/CeO_2	0.1	3.0	0.61
Rh(N)/CeO_2	0.3	6.9	0.47
Rh(N)/CeO_2	1.0	14.1	0.29
Rh(N)/CeO_2[b]	1.0	11.5	0.24
Rh(N)/CeO_2[c]	1.0	9.4	0.19
Rh(N)/CeO_2	2.8	26.3	0.19
Rh(Cl)/CeO_2	1.1	15.4	0.28
Rh(A)/CeO_2	1.0	14.7	0.30
Rh(C)/CeO_2	1.0	15.1	0.31

[a] Rh/CeO_2 obtained from uncalcined precatalysts. [b] Obtained from Rh^{3+}(N)/CeO_2 calcined at 400 °C. [c] Obtained from Rh^{3+}(N)/CeO_2 calcined at 700 °C.

Table 8 Coke deposition on spent Rh catalysts after 5 h of ESR at 350 °C evaluated by TGA in air[a]

spent catalyst	amount of coke formed		
	(mg/g cat.)	(mol/mol Rh)	(mol/mol surf. Rh)
Rh(N)/SiO_2	29.4	25.2	–
Rh(N)/γ-Al_2O_3	24.5	21.0	–
Rh(N)/MgO	13.6	11.7	–
Rh(N)/ZrO_2	5.2	4.5	–
Rh(N)/La_2O_3	14.6	12.5	–
Rh(N)/Y_2O_3	6.7	5.7	–
Rh(N)/TiO_2	11.2	9.6	–
Rh(N)/ZnO	10.7	9.2	–
Rh(N)/CeO_2	0.6	0.5	1.8
Rh(Cl)/CeO_2	0.6	0.5	1.9
Rh(A)/CeO_2	0.8	0.7	2.3
Rh(C)/CeO_2	n.d.[b]	–	–
Rh(C)/CeO_2[c]	1.1	0.9	3.0

[a] 1 % Rh loading in precatalysts. [b] Not detected. [c] After 5 h of ESR at 300 °C.

strengthened and thus the TPR processes can produce smaller supported Rh particles from surface Rh oxides as well as supported bulk-like Rh_2O_3.

The nature of the interaction of metal precursor with support also determines the catalytic properties of supported metal catalysts in ESR. It is necessary to mention that we chose the reduction temperature at 400 °C for all precatalysts and calcined precatalysts prior to the ESR reaction according to the highest desired reaction temperature. This reduction temperature may be inferior to those of certain surface Rh oxides due to the strong Rh^{3+}-support interaction mentioned above. However, this would not affect the actual investigation of catalytic properties with the Rh active sites in low-temperature ESR. It is reasonable to reckon that the states of the Rh active sites in ESR rely on the reaction temperature. Even if certain surface Rh oxides undergo higher-temperature reduction, the resulting supported Rh particles, once oxidized during ESR at 400 °C or below, cannot restore their active states at the identical temperature. Therefore, we gave up using higher reduction temperatures for precatalysts and calcined precatalysts. The catalytic contributions of these surface Rh oxides were ignored in this work.

H_2 chemisorption of fresh CeO_2-supported Rh catalysts In Table 7 are presented the results of H_2 chemisorbed on different Rh precursor-derived fresh CeO_2-supported Rh catalysts. The apparent H/Rh value can be used to represent the dispersion of zero-valent Rh on the support or the reduction degree of surface Rh for a supported Rh catalyst. On Rh(N)/CeO_2 obtained from uncalcined Rh^{3+}(N)/CeO_2, the apparent H/Rh value decreased from 0.61 to 0.19 with increasing Rh loading from 0.1 to 2.8 %. This relationship implies that increasing the Rh loading on CeO_2 is susceptible to render the Rh metal less dispersed or the Rh particle size enlarged, which confirms that the specific catalytic activity of Rh/CeO_2 for the C_2H_5OH conversion increases with increasing dispersion of Rh metal. However, on Rh(N)/CeO_2 obtained from Rh^{3+}(N)/CeO_2 calcined at 400 and 700 ^oC, the apparent H/Rh values were 0.24 and 0.19, respectively. This may imply that the calcination of Rh^{3+}(N)/CeO_2 may lead to incomplete reduction of Rh^{3+} on CeO_2 due to the strong Rh^{3+}-CeO_2 interaction, assuming that the Rh particle size remains unchanged. Some similar situations with irreducible supported metals at given reduction temperatures are well documented for oxide-supported metal catalysts because of strong metal-support interaction after calcination.[99-101] The incomplete reduction of Rh^{3+} actually lowers the active Rh loading on CeO_2. Either the calcination or the incomplete reduction of Rh^{3+} can lead to the formation of smaller supported Rh particles, which is in line with the decreased C_2H_5OH conversion, CH_3CHO transformation and H_2 yield in low-temperature ESR over the catalysts obtained from Rh^{3+}(N)/CeO_2 calcined at 400 and 700 ^oC (Table 5). On Rh/CeO_2 derived from any of the four Rh precursors with a 1 % Rh loading, the apparent H/Rh value was 0.28-0.31, which hints that the dispersion of Rh metal or the Rh particle size on CeO_2 is little affected by the Rh precursor. This further accounts for that the poorer catalytic performance of Rh(Cl)/CeO_2 for ESR arises from the detrimental effect of Cl, regardless of the dispersion of Rh metal on CeO_2. This is also in agreement with the comparable C_2H_5OH conversions and H_2 yields in low-temperature ESR over Rh(N)/CeO_2, Rh(A)/CeO_2 and Rh(C)/CeO_2 (Table 3).

TGA of spent Rh catalysts TGA in air can be used to evaluate the amounts of coke formed on solid catalysts during ESR through combustion of carbonaceous species. In Table 8 are compared the amounts of coke deposited on all the spent Rh catalysts studied after 5 h of ESR at 350 ^oC calculated from TGA data. Larger amounts of coke (10.7-29.4 mg/g cat.) were formed on Rh(N)/SiO_2, Rh(N)/γ-Al_2O_3, Rh(N)/MgO, Rh(N)/La_2O_3, Rh(N)/TiO_2 and Rh(N)/ZnO, while smaller amounts of coke (6.7 mg/g cat. and below) were observed on Rh(N)/ZrO_2, Rh(N)/Y_2O_3 and Rh/CeO_2. Above all on the Rh/CeO_2 catalysts, remarkably tiny amounts of coke (0.8 mg/g cat. and below) were noted. These comparative results are consistent with the reported stronger ability of CeO_2 to suppress coke deposition in ESR.[47-50] The comparative amounts of coke deposited on the spent oxide-supported Rh catalysts show that Rh/CeO_2 is

of a significant advantage over the other Rh/oxide catalysts in the resistance against coking during low-temperature ESR, which can reasonably predict a better catalytic stability of Rh/CeO_2 than that of the other Rh/oxide catalysts. The strong resistance of Rh/CeO_2 against coking consists in a high oxygen storage capacity of CeO_2.[102,103]

Of all the spent Rh/CeO_2 catalysts after 5 h of ESR at 350 ^oC, the amount of coke formed on $Rh(C)/CeO_2$ was not detectable, while those on the other Rh/CeO_2 catalysts attained to 1.8-2.3 mol/surf. mol Rh. For spent $Rh(C)/CeO_2$ after 5 h of ESR at 300 ^oC, the amount of coke deposited went up to 3.0 mol/mol surf. Rh. The results apparently show that coking on Rh/CeO_2 is sensitive to the ESR temperature and low temperatures are favourable to coking, in conformity with thermodynamic analysis of ESR.[88,89] On the other hand, the results indicate that use of Rh/CeO_2 can suppress coke deposition during ESR at temperatures as low as 350 ^oC depending on the Rh precursor and the precatalyst pretreatment. At 300 ^oC, Rh/CeO_2 has a high probability of blockage of Rh metal sites by coke deposition during ESR. At 350 ^oC, the probability of blockage is negligible for $Rh(C)/CeO_2$ and still present for $Rh(N)/CeO_2$, $Rh(Cl)/CeO_2$ and $Rh(A)/CeO_2$. Coking on Rh/CeO_2 is in line with the catalytic stability of Rh/CeO_2 at 350 ^oC, in correlating the amount of coke formed with the extent of catalyst deactivation in ESR on stream over $Rh(N)/CeO_2$, $Rh(A)/CeO_2$ and $Rh(C)/CeO_2$. The strong resistance of $Rh(C)/CeO_2$ against coking may be related to the unique structural and surface properties of the CeO_2-supported Rh metal particles derived from $Rh_4(CO)_{12}$, which make a distinct difference from those of the CeO_2-supported Rh metal particles derived from the other Rh precursors. When using $Rh(C)/CeO_2$ as a catalyst, ESR has turned out to be strongly kinetically controlled in favour of suppression of coking on the catalyst in this work. The relevant aspects need in-depth investigation in the future.

Rh 3d XPS analysis of CeO_2-supported Rh catalysts Rh 3d XPS was used to determine the oxidation valence of surface Rh and the ratio among various surface Rh species with different valences in Rh/CeO_2. Figs. 12 and 13 show the Rh 3d XPS spectra of different Rh precursor-derived CeO_2-supported Rh catalysts before and after 5 h of ESR at 350 ^oC. Before XPS experiments, the fresh catalyst samples $Rh(N)/CeO_2$, $Rh(A)/CeO_2$ and $Rh(C)/CeO_2$ were exposed to air at 21 ^oC for 5 h. The spectra of all the three fresh catalyst samples presented a pair of symmetric peaks at 306.7-307.4 and 311.4-312.1 eV, which are asigned to Rh^0 via curve-fitting (see Fig. 12 and Table 9).[104,105] The results clearly indicate that the surface Rh of all the three fresh catalysts is zero-valent and that the CeO_2-supported Rh metal particles are stable enough not to be oxidized in air at 21 ^oC. The spectrum of spent $Rh(N)/CeO_2$ displayed a pair of symmetric peaks at 308.5 and 313.2 eV while that of spent $Rh(A)/CeO_2$ exhibited a pair of symmetric ones at 306.9 and 311.6 eV. These two pairs of peaks correspond to the binding

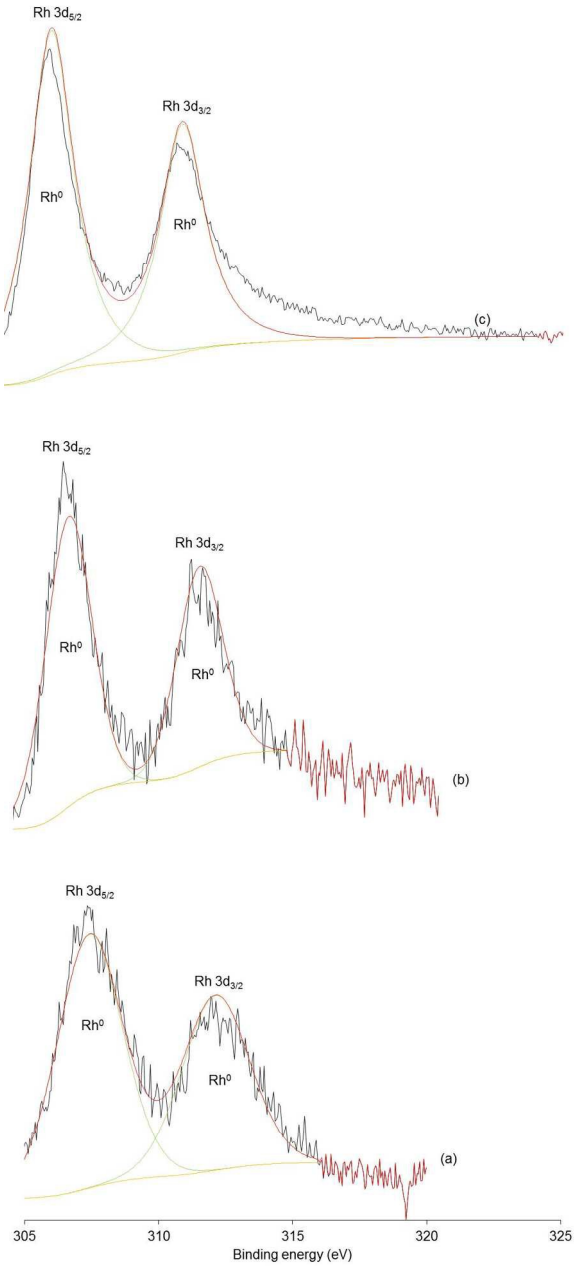

Fig. 12 Rh 3d XPS spectra of (a) Rh(N)/CeO_2, (b) Rh(A)/CeO_2 and (c) Rh(C)/CeO_2. The black and red curves stand for the raw experimental data and the sum of the Gaussian components, respectively. The peak intensity is adjusted to facilitate the comparison among the different samples.

energies of Rh^+ and of Rh^0 via curve-fitting (see Fig. 13 and Table 9), respectively, which postulates that the supported Rh metal particles are oxidized to Rh^+ for Rh(N)/CeO_2 and remain as Rh^0 for Rh(A)/CeO_2 during ESR at 350 ^oC. For spent Rh(C)/CeO_2, two pairs of peaks can be fitted out at 307.3 and 312.0, 308.7 and 313.5 by deconvolution (see Fig. 13 and Table 9), which are attributed to a mixture of Rh^0 and Rh^+. This postulates part oxidation of the supported Rh metal particles to Rh^+ for Rh(C)/CeO_2 during ESR

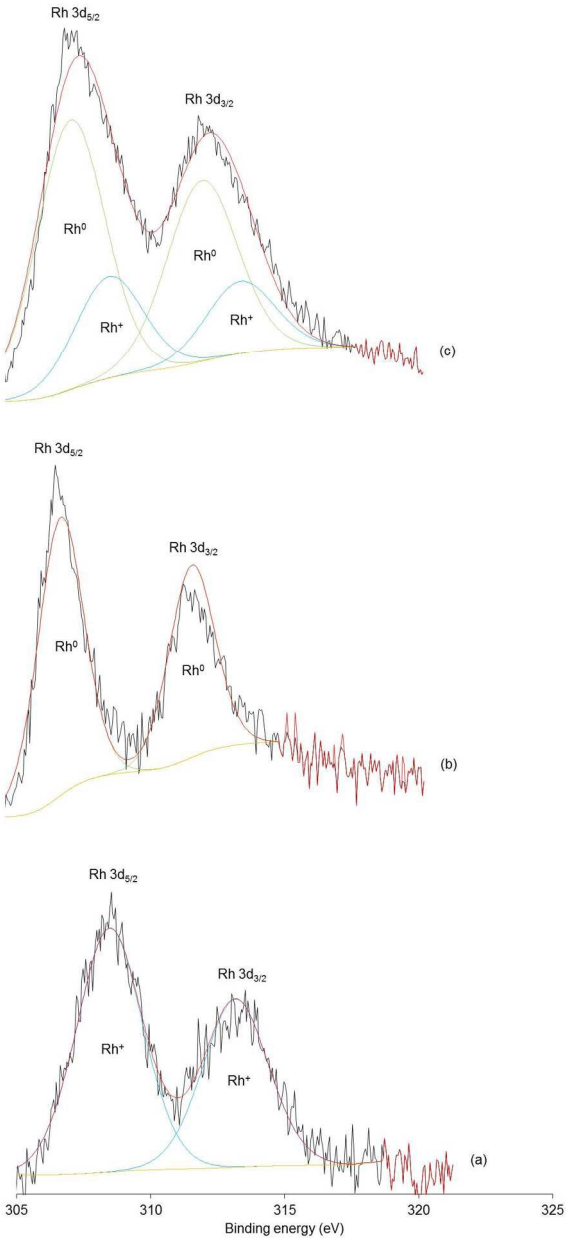

Fig. 13 Rh 3d XPS spectra after 5 h of ESR at 350 °C of (a) Rh(N)/CeO_2, (b) Rh(A)/CeO_2 and (c) Rh(C)/CeO_2. The black and red curves stand for the raw experimental data and the sum of the Gaussian components, respectively. The peak intensity is adjusted to facilitate the comparison among the different samples.

Table 9 Valences of surface Rh in CeO_2-supported Rh catalysts estimated by XPS

catalyst	before ESR		after ESR	
	Rh^0 %	Rh^+ %	Rh^0 %	Rh^+ %
Rh(N)/CeO_2	100	0	0	100
Rh(N)/CeO_2[a]	50	50	–	–
Rh(N)/CeO_2[b]	60	40	–	–
Rh(A)/CeO_2	100	0	100	0
Rh(C)/CeO_2	100	0	73	27

[a] Obtained from Rh^{3+}(N)/CeO_2 calcined at 400 °C. [b] Obtained from Rh^{3+}(N)/CeO_2 calcined at 700 °C.

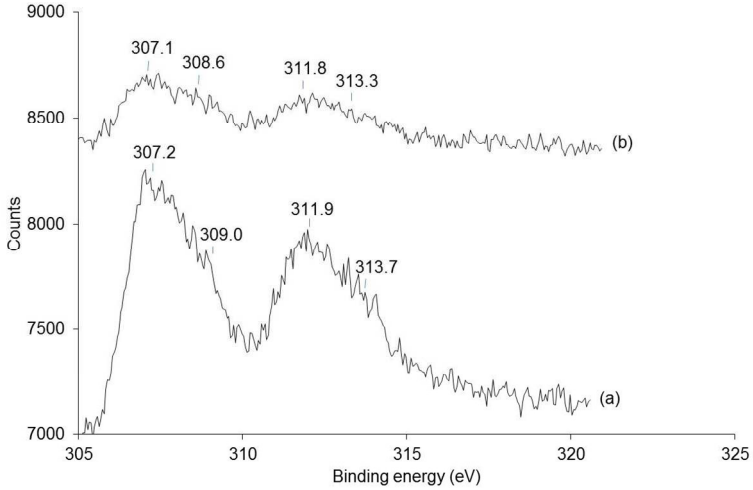

Fig. 14 Rh 3d XPS spectra of $Rh(N)/CeO_2$ obtained from $Rh^{3+}(N)/CeO_2$ calcined at (a) 400 °C (b) 700 °C.

at 350 °C.

However, the Rh 3d XPS spectra of two fresh catalyst samples obtained from $Rh^{3+}(N)/CeO_2$ calcined at 400 and 700 °C (Fig. 14), present two pairs of peaks that can be fitted out by deconvolution (see ESI and Table 9), which are attributed to a mixture of Rh^0 and Rh^+. This suggests that the surface Rh^{3+} in H_2 at 400 °C is incompletely reduced to Rh^0 with the formation of a large fraction of Rh^+ because of the strong Rh^{3+}-CeO_2 interaction. At the same time, the peak intensity of the catalyst sample obtained from $Rh^{3+}(N)/CeO_2$ calcined at 700 °C was much lower than that at 400 °C under equivalent measurement conditions, assuming that the calcination at 700 °C results in a reduced fraction of surface Rh^{0-1}. This may be caused by a heavy sintering (decrease in the surface area) of CeO_2 upon calcination at 700 °C.[97] In all the Rh 3d XPS spectra shown in Figs. 12-14, no peaks due to Rh^{2+} and Rh^{3+} other than those of Rh^0 and Rh^+ can be fitted out by deconvolution.

The XPS results in Fig. 14 are in accordance with those of the catalytic evaluation, TPR and H_2 chemisorption of the same catalysts obtained by calcination of $Rh^{3+}(N)/CeO_2$. At this stage, however, it is difficult to verify the assumption that the dispersion of Rh metal on CeO_2 increases with increasing calcination temperature by TEM. Due to the strong influence of the dark background of small CeO_2 particles in TEM images, it is difficult to properly measure Rh particle sizes and thus acquire accurate Rh particle size distributions.[106] On the other hand, CeO_2 has been recognized as a material for strong metal-support interaction (SMSI).[106] CeO_2-supported noble metal catalysts are long known to exhibit SMSI effects.[106,107] Possibly because of the Rh^{3+}-CeO_2 SMSI at high temperatures, the Rh^{3+} is partly buried or wrapped by CeO_2 particles after the calcination like in other CeO_2-supported noble metal systems,[106,107] which limits the access of H_2 to the supported Rh^{3+} in TPR and the access of C_2H_5OH to the active Rh sites in ESR.

From Table 9, the supported Rh^0 is fully oxidized to Rh^+ for $Rh(N)/CeO_2$, fully retained for $Rh(A)/CeO_2$ and partly oxidized to Rh^+ for $Rh(C)/CeO_2$ after 5 h of ESR at 350 ^oC. Since none of these three catalysts deactivates but all of them are highly active instead for H_2 generation from ESR when the reaction proceeds to 5 h (Figs. 5-7), it is difficult to rule out the possibility that both the supported Rh^0 and Rh^+ participate in catalysis or promotion for H_2 generation from ESR. It is unlikely that oxidation of the supported Rh^0 to Rh^+ causes the catalyst deactivation on Rh/CeO_2 during ESR.

To our knowleadge, the roles of Rh sites with different valences in supported Rh catalysts in ESR remain unclear. By contrast, the roles of Co sites with different valences in supported Co catalysts in ESR have been increasingly concerned about in recent years.[108-112] O' Shea et al. investigated the evolution of Co_3O_4 under *operando* conditions with P-XRD, and observed that Co_3O_4 was not active but the evolved material with CoO and Co^0 was active and selective in ESR.[24] To identify the roles of Co^0 and Co^{2+} in ESR, Tuti and Pepe investigated bulk Co_3O_4 (both oxidized and reduced), Co/MgO and CoO/MgO with TPR.[108] They suggested that Co^0 is mainly responsible for ESR while Co^{2+} is active for EDA. Hyman and Vohs studied the reaction of C_2H_5OH on metallic and oxidized Co single crystal surfaces using TPD and XPS, to determine the dependence of the reaction pathways on the Co oxidation state.[109] They found that the primary reaction for ethoxide species on Co^0 was decarbonylation producing CO, H_2 and carbon, CoO_x that predominantly contained Co^{2+} was selective for dehydrogenation of ethoxide groups producing CH_3CHO, and more highly oxidized Co that contained both Co^{2+} and Co^{3+} was active for complete oxidation of C_2H_5OH producing CO, CO_2, and H_2O. Passos et al. examined the effect of the balance between Co^0 and Co^{2+} on the catalytic activity of Co/Al_2O_3 for ESR using time-resolved *in situ* X-ray absorption spectroscopy.[110] They correlated the catalytic performance with the ratio of Co^{2+}/Co^0, and pointed out that control of Co^{2+}/Co^0 ratio helps maintain the balance between C_2H_5OH conversion and C oxidation, resulting in stable catalysts. Wang's group studied the roles of Co^0 and Co^{2+} in ESR over oxide-supported Co catalysts.[111,112] For Co/MgO, they observed with the aid of TPR and *in situ* XPS that Co^0 is much more active than Co^{2+} for C_2H_5OH conversion, C-C cleavage and WGS, whereas C_2H_5OH decomposition to CH_4 is dominant on Co^{2+}.[111] For Co/ZrO_2, they concluded with TPR, *in situ* XPS and theoretical density functional theory calculations that Co^0 is mainly responsible for ACSR, while Co^{2+} plays a key role in converting C_2H_5OH into $(CH_3)_2CO$ via dehydrogenation and condensation/ketonization.[112] All these studies clearly indicate that both Co^0 and Co^{2+} in supported Co catalysts act as active sites for different reaction pathways during ESR. It appears that an appropriate Co^{2+}/Co^0 ratio may lead to good catalytic performance and stability in ESR. Because of the similarity between Co and noble metal catalysts in the activity for C-C bond cleavage and in the selectivity to H_2, CO_2 and CH_4 in ESR,[47,113-118] different catalytic roles of Rh sites with different valences in ESR deserve to

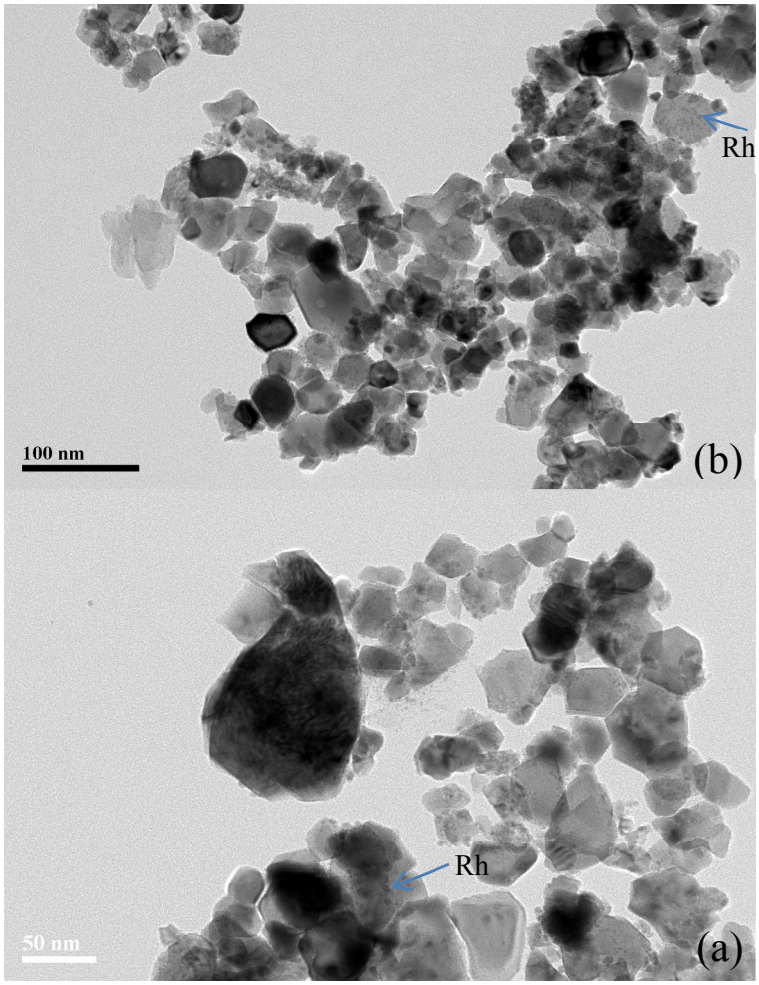

Fig. 15 TEM images of Rh(N)/CeO_2 (a) before and (b) after 25 h of ESR at 350 °C.

be considered.

Our XPS results suggest that the different Rh precursors on CeO_2 lead to different extents of oxidation of Rh metal particles during ESR. Although the Rh/CeO_2 catalysts derived from $Rh(NO_3)_3 \cdot xH_2O$, $Rh(acac)_3$ and $Rh_4(CO)_{12}$ by H_2 treatment at 400 °C have much the same Rh dispersion on CeO_2 and the similar initial activity for ESR, the natures of the interaction between Rh metal particles and CeO_2 may be discrepant in the three cases, so that Rh(N)/CeO_2, Rh(A)/CeO_2 and Rh(C)/CeO_2 behave differently against Rh oxidation as observed in this work. More recently, Simson et al. reported through *in situ* XPS measurements that during ESR at 650 °C, a 4 %Rh/Al_2O_3/ZrO_2 monolith catalyst underwent a gradual Rh oxidation.[119] Coronel et al. showed by a comparative XPS study that after ESR at 500 °C, Rh^0 was oxidized to Rh^{n+} in 0.6 %Rh/La_2O_3(40 %)-SiO_2 and 0.6 %Rh/CeO_2-La_2O_3(10 %)-SiO_2 catalysts, and Rh^0 remained unchanged in a 0.6 %Rh/La_2O_3(15 %)-SiO_2 catalyst.[68] These results demonstrate that supported Rh has a propensity to be oxidized under ESR conditions, depending on the nature of the Rh-support interaction or the dispersion of Rh metal particles.

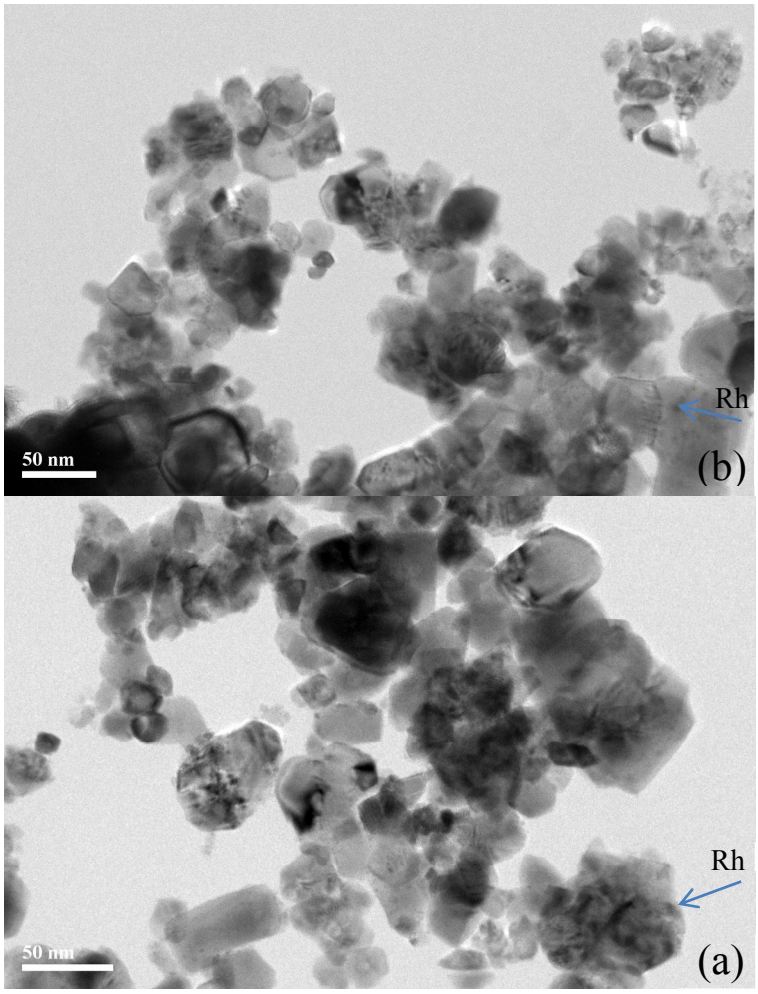

Fig. 16 TEM images of Rh(A)/CeO_2 (a) before and (b) after 25 h of ESR at 350 ^oC.

TEM analysis of CeO_2-supported Rh catalysts. TEM was used to observe the microscopic morphology of CeO_2-supported Rh metal particle catalysts. Figs. 15 and 16 show the TEM pictures of Rh(N)/CeO_2 and Rh(A)/CeO_2 before and after 25 h of ESR at 350 ^oC. Roughly, the particle size of CeO_2 was estimated to be 6-40 nm. The small dark spots were identified as the images of Rh metal particles on the CeO_2 support by energy dispersive X-ray analysis (EDX). It was observed that the Rh metal particles were well dispersed on the CeO_2 surface with a size of 2-5 nm in the cases of both Rh(N)/CeO_2 and Rh(A)/CeO_2. Due to the strong influence of the CeO_2 dark background, it is difficult to properly measure the particle sizes of both Rh metal and CeO_2 and thus acquire their particle size distributions. From the comparative particle sizes of both Rh metal and CeO_2 before and after ESR, there were no visible particle growths occurring after ESR for both Rh metal and CeO_2 in the cases of both Rh(N)/CeO_2 and Rh(A)/CeO_2. The observations suggest that sintering of Rh metal and CeO_2 particles in Rh/CeO_2 does not take place under the ESR conditions. Thus, the possibility that sintering of Rh metal and CeO_2 particles in Rh/CeO_2 leads

to the catalyst deactivation during ESR at 350 ^{o}C can be ruled out.

XRD analysis of CeO_2-supported Rh catalysts. XRD was used to check the phase structure of CeO_2 in Rh/CeO_2. In ESI are shown the XRD patterns of Rh(N)/CeO_2 and Rh(A)/CeO_2 before and after 25 h of ESR at 350 ^{o}C. Since the 1 % Rh loading in Rh/CeO_2 was rather low, the diffraction peaks of Rh metal particles did not appear. The diffraction peaks of CeO_2 with fluorite structure remained unchanged in intensity and width after ESR. The results demonstrate that sintering of CeO_2 particles in Rh/CeO_2 does not occur under the ESR conditions, in agreement with the TEM observations. Thus, it is confirmed that the possibility that sintering of CeO_2 particles in Rh/CeO_2 leads to the catalyst deactivation during ESR at 350 ^{o}C can be also ruled out.

Conclusions

The following can be concluded from the whole work.

(1) Various types of oxides themselves are catalytically active for H_2 generation from the ESR process though the H_2 yield is low. The acidic oxide γ-Al_2O_3 favours EDE followed by ED to generate H_2, the basic oxide MgO catalyzes EDA to release H_2, the weakly acidic oxide SiO_2 catalyzes EDA to give H_2 to a small extent, and the redox oxide CeO_2 eases WGS as well as EDA, EDAC, ASR and ACSR to produce H_2. The presence of Rh on oxides greatly enhances the catalytic activity for all the reaction pathways involved in ESR.

(2) Rh(N)/CeO_2, Rh(N)/ZrO_2 and Rh(N)/γ-Al_2O_3 are generally advantageous in H_2 production from low-temperature ESR. Rh(N)/CeO_2, Rh/γ-Al_2O_3, Rh/MgO and Rh/SiO_2 are advantageous over Rh/ZrO_2, Rh/La_2O_3, Rh/Y_2O_3, Rh/TiO_2 and Rh/ZnO in AD and ASR during low-temperature ESR. Rh/CeO_2 is most active among all the oxide-supported Rh catalysts studied for WGS during low-temperature ESR.

(3) Likely due to the detrimental influence of Cl retained in the CeO_2 lattice on catalysis, Rh(Cl)/CeO_2 has poorer catalytic performance than Rh(N)/CeO_2, Rh(A)/CeO_2 and Rh(C)/CeO_2 in H_2 generation from low-temperature ESR.

(4) For Rh/CeO_2, the efficiency of H_2 production increases with decreasing Rh loading, the 0.1 % Rh loading enables slight decrease in the selectivity to CH_4, but Rh loadings below 1 % disable complete removal of CO from low-temperature ESR. The 1 % Rh loading appears optimal for H_2 generation from low-temperature ESR.

(5) Calcination of Rh^{3+}/CeO_2 leads to decreases in the H_2 yield and selectivity to CH_4 and an increase in

the selectivity to CO in low-temperature ESR, which may be due to reduced amounts of surface Rh^0 caused by the strong Rh^{3+}-CeO_2 interaction. The strong Rh^{3+}-CeO_2 interaction at high temperatures such as 700 ^oC can render the Rh^{3+} to be partly buried or wrapped by CeO_2 particles after the calcination, which limits the access of H_2 to the supported Rh^{3+} in TPR and the access of C_2H_5OH to the active Rh sites in ESR.

(6) Rh(C)/CeO_2 has stable catalytic performance during at least 24 h of ESR at 350 ^oC with a CO-free H_2 yield of 4 mol/mol C_2H_5OH. In contrast, Rh(N)/CeO_2 and Rh(A)/CeO_2 deactivate gradually as the reaction proceeds under equivalent conditions. The discrepancy in the catalytic stability can be related to the different amounts of coke formed on these catalysts which cause the catalyst deactivation to a different extent. Other factors causing the catalyst deactivation such as oxidation of the Rh metal particles and sintering of the Rh metal particles and CeO_2 in Rh/CeO_2 during ESR, can be ruled out.

(7) Both CeO_2-supported Rh^0 and Rh^+ may participate in catalysis for ESR to produce H_2, based on the fact that the catalytic reaction is observed to proceed efficiently in the presence of either CeO_2-supported Rh^0 or Rh^+.

(8) H_2 generation from low-temperature ESR is strongly kinetically controlled in the presence of Rh/CeO_2. Rh/CeO_2 promotes H_2 production via ASR, ACSR and WGS at 300 ^oC, and via ASR, ACSR, MD, steam reforming of adsorbed CH_x (x = 1-3) and WGS at 400 ^oC.

Experimental

$Rh_4(CO)_{12}$ and $Rh(acac)_3$ were supplied by Strem. $Rh(NO_3)_3 \cdot xH_2O$, $RhCl_3 \cdot xH_2O$, silica gel (SiO_2, Merck), γ-Al_2O_3, $Mg(OH)_2$ (95 %), CeO_2 (99.9 %), ZrO_2 (99.99 %), La_2O_3 (99.999 %), Y_2O_3 (99.99 %), TiO_2 (99.99 %), ZnO (99.99 %) and other reagents were purchased from Aldrich. MgO was derived from $Mg(OH)_2$ by 4 h of calcination in flowing air at 400 ^oC, which was confirmed by the structural transition in P-XRD (see ESI). H_2 and Ar gases used in experiments had a purity of 99.999 %.

The above Rh compounds and metal oxides were used as precursors and supports to prepare oxide-supported Rh precatalysts and catalysts. The physical properties of the oxides were determined by N_2 adsorption-desorption, as shown in Table 10. In preparing precatalysts, the oxides were previously dried at 110 ^oC in air overnight. Precatalysts from $Rh_4(CO)_{12}$ were obtained through impregnation in dry hexanes under Ar as described previously.[40] Precatalysts from $Rh(acac)_3$ were obtained through impregnation in dry toluene under Ar following a similar procedure.[40] After evacuation of organic solvents, the precatalysts were stored in Schlenk tubes under Ar. Precatalysts from inorganic salts were obtained through incipient wetting. After removal

Table 10 Physical properties of supports determined from N_2 adsorption-desorption

support	BET surface area (m^2/g)	pore volume (ml/g)	pore diameter (Å)
SiO_2	312.0	1.048	120.5
γ-Al_2O_3	146.8	0.207	34.2
MgO	10.5	0.091	35.6
CeO_2	7.7	0.035	40.5
ZrO_2	5.0	0.046	35.6
La_2O_3	4.2	0.015	174.2
TiO_2	4.3	0.021	25.6
ZnO	14.7	0.062	28.6
Y_2O_3	5.2	0.026	231.8

of water under vacuum, the precatalysts were dried under vacuum (10^{-2} torr) overnight at 21 ^oC and stored in a vacuum dessicator. The Rh loading in the precatalysts was set at 1 % unless mentioned where necessary. The $Rh_4(CO)_{12}$-derived CeO_2-supported Rh precatalysts and catalysts are denoted as $Rh_4(C)/CeO_2$ and $Rh(C)/CeO_2$, the $Rh(acac)_3$-derived CeO_2-supported Rh precatalysts and catalysts as $Rh^{3+}(A)/CeO_2$ and $Rh(A)/CeO_2$, the $Rh(NO_3)_3 \cdot xH_2O$ -prepared CeO_2-supported Rh precatalysts and catalysts as $Rh^{3+}(N)/CeO_2$ and $Rh(N)/CeO_2$, the $RhCl_3 \cdot xH_2O$ -prepared CeO_2-supported Rh precatalysts and catalysts as $Rh^{3+}(Cl)/CeO_2$ and $Rh(Cl)/CeO_2$. For the purpose of studying the strong metal-support interaction, $Rh^{3+}(N)/CeO_2$ was subjected to 4 h of calcination in air at 400 and 700 ^oC, respectively.

ESR catalysts were tested using a customized five channel fixed-bed quartz reactor from Bel Japan Inc that was connected to a Varian GP 380 gas chromatographe (GC). Four of the five reaction tubes were used for catalyst tests, with one serving as a reference for blank tests. Precatalysts or calcined precatalysts (0.15 g each) were reduced in H_2 using a heating program with 10 ^oC/min from 21 to 400 ^oC and holding at 400 ^oC for 30 min in the reaction tubes and flushed with Ar for 30 min while cooled to 250 ^oC, followed by introduction of a reactant mixture with Ar. A liquid mixture of C_2H_5OH and H_2O (1 : 3 volumetric ratio or 1 : 10 molar ratio) at a flow rate of 0.005 ml/min was fed into the vaporizer at 170 ^oC with Ar at a flow rate of 39 ml/min before admission to the reaction tubes (Ar : C_2H_5OH : H_2O = 49 : 1 : 10 molar ratio, 1.7 mol% C_2H_5OH). The reactant composition with a C_2H_5OH : H_2O molar ratio of 1 : 10 was similar to a bioethanol stream from biomass fermentation. The Ar : (C_2H_5OH + H_2O) molar ratio and GHSV amounted to 4.6 and 26200/h (namely 17700 ml/g/h), respectively. For a general test of catalytic performance as a function of reaction temperature, the ESR reaction was consecutively run from 250 to 500 ^oC or 600 ^oC and each reaction temperature was held for 30 min. The reaction products were analyzed twice on line by gas chromatography after 10 min of reaction at each reaction temperature. For an assessment of catalytic stability, the ESR reaction was operated at a couple of fixed temperatures.

The GC was equiped with two channels connected to two thermal conductivity detectors, respectively. One was made up of a molecular sieve 5 Å column using Ar as carrier gas for analysis of H_2 and CO, the other of a Hayesep Q column using He as carrier gas for analysis of CO_2, CH_4, C_2H_4, C_2H_6, C_2H_5OH, CH_3CHO, $(CH_3)_2CO$ and H_2O.

Conversion of C_2H_5OH, selectivity to a C-containing product, selectivity to H_2 and yield of H_2 were estimated according to the following formulae:

$$X(C_2H_5OH)\ \% = \left(1 - \frac{2(\text{mol } C_2H_5OH)}{2(\text{mol } C_2H_5OH) + \sum x(\text{mol } C_xH_yO_z)}\right) \times 100$$

$$S(C_xH_yO_z)\ \% = \frac{x(\text{mol } C_xH_yO_z)}{\sum x(\text{mol } C_xH_yO_z)} \times 100$$

$$S(H_2)\ \% = \frac{2(\text{mol } H_2)}{2(\text{mol } H_2) + \sum y(\text{mol } C_xH_yO_z)} \times 100$$

$$Y(H_2) = X(C_2H_5OH) \times S(H_2) \times 6$$

where $C_xH_yO_z$ stands for a C- containing product or H-containing organic product. $X(C_2H_5OH)$ was gained based on unreacted C_2H_5OH and all detected C-containing products, $S(C_xH_yO_z)$ on all detected C-containing products, and $S(H_2)$ on H_2 and all detected H-containing organic products. $Y(H_2)$ was expressed in terms of the moles of H_2 produced per mole of C_2H_5OH. Blank tests verified the absence of gas phase reactions. Under the reaction conditions used in this work, only H_2, CO, CO_2, CH_4, C_2H_4, C_2H_6, CH_3CHO and $(CH_3)_2CO$ were detected as the products.

Surface areas of supports were measured by N_2 adsorption-desorption on a Quantachrome Autosorb-6B analyzer.

Reductive behaviour of precatalysts or calcined precatalysts with a 1 % Rh loading was studied by TPR on a Thermo Scientific TPROD 1100 instrument. Prior to TPR experiments, all precatalyst and calcined precatalyst samples except the $Rh_4(C)/CeO_2$ sample were dried under vacuum at 21 ^oC for 2 h, the $Rh_4(C)/CeO_2$ sample was oxidized in air followed by 2 h of drying under vacuum (see ESI). A TPR profile was obtained by passing 5 % H_2/Ar at a flow rate of 50 ml/min through a sample of 0.10 g from 30 to 800 or 850 ^oC using a heating rate of 10 ^oC/min. H_2 consumption during TPR was recorded in thermal conductivity signals. Quantification of H_2 consumed was done by calibration with the aid of TPR profiles of known amounts of bulk CuO. H_2 consumption was obtained from the integrated peak area relative to the average calibration value.

Apparent H/Rh values were determined by H_2 pulse chemisorption, as stated previously.[40]

Amounts of carbon formed on catalysts during ESR were evaluated by TGA in air, as stated previously.[40]

Rh oxidation states in CeO_2-supported Rh catalysts were determined by XPS, as stated previously.[40]

Microscopic images of CeO_2-supported Rh catalysts were observed by TEM, as stated previously.[40]

Phase structures of solid materials were analyzed by XRD on a Siemens D5005 spectrometer.

Rh contents in precatalysts and catalysts were determined by the inductively coupled plasma (ICP) technique on a Varian Vista-MPX CCD simultaneous ICP-OES spectrograph.

Acknowledgment

We acknowledge the Science and Engineering Research Council (SERC) of the Agency for Science, Technology and Research (A*STAR) for financial support.

References

1 I. Fishtik, A. Alexander, R. Datta and D. Geana, *Int. J. Hydrogen Energy,* 2000, **25,** 31-45.

2 P. D. Vaidya and A. E. Rodrigues, *Chem. Eng. J.,* 2006, **117,** 39-49.

3 A. Erdõhelyi, J. Raskó, T. Kecskés, M. Tóth, M. Dömök and K. Baán, *Catal. Today,* 2006, **116,** 367-376.

4 H.-S. Roh, Y. Wang, D. L. King, A. Platon and Y.-H. Chia, *Catal. Lett.,* 2006, **108,** 15-19.

5 B. Zhang, X. Tang, Y. Li, Y. Xu and W. Shen, *Int. J. Hydrogen Energy,* 2007, **32,** 2367-2373.

6 A. C. Basagiannis, P. Panagiotopoulou and X. E. Verykios, *Top. Catal.,* 2008, **51,** 2-12.

7 E. B. Pereira, N. Homs, S. Marti, J. L. G. Fierro and P. Ramirez de la Piscina, *J. Catal.,* 2008, **257,** 206-214.

8 F. Auprêtre, C. Descorme and D. Duprez, *Catal. Commun.,* 2002, **3,** 263-267.

9 D. K. Liguras, D. I. Kondarides and X. E. Verykios, *Appl. Catal. B.,* 2003, **43,** 345-354.

10 F. Frusteri, S. Freni, V. Chiodo, L. Spadaro, O. Di Blasi, G. Bonura and S. Cavallaro, *Appl. Catal. A.,* 2004, **270,** 1-7.

11 A. N. Fatsikostas and X. E. Verykios, *J. Catal.,* 2004, **225,** 439-452.

12 J. Comas, F. Mariño, M. Laborde and N. Amadeo, *Chem. Eng. J.,* 2004, **98,** 61-68.

13 A. Aboudheir, A. Akande, R. Idem and A. Dalai, *Int. J. Hydrogen Energy,* 2006, **31,** 752-761.

14 C. C. R. S. Rossi, C. G. Alonso, O. A. C. Antunes, R. Guirardello and L. Cardozo-Filho, *Int. J. Hydrogen Energy,* 2009, **34,** 323-332.

15 A. Haryanto, S. Fernando, N. Murali and S. Adhikari, *Energy. Fuels,* 2005, **19,** 2098-2106.

16 A. Bshish, Z. Yaakob, B. Narayanan, R. Ramakrishnan and A. Ebshish, *Chem. Papers,* 2011, **65,** 251-

266.

17 J. L. Contreras, J. Salmones, J. A. Colín-Luna, L. Nuño, B. Quintana, I. Córdova, B. Zeifert, C. Tapia and G. A. Fuentes, *Int. J. Hydrogen Energy,* 2014, **39,** 18835-18853.

18 K. Otsuka, M. Hatano and A. Morikawa, *J. Catal.,* 1983, **79,** 493-496.

19 T. Bunluesin, R. J. Gorte and G. W. Graham, *Appl. Catal. B.,* 1998, **15,** 107-114.

20 S. Hilaire, X. Wang, T. Luo, R. J. Gorte and J. Wagner, *Appl. Catal. A.,* 2001, **215,** 271-278.

21 J. Llorca, P. Ramirez de la Piscina, J. Sales and N. Homs, *Chem. Commun.,* 2001, 641-642.

22 J. P. Breen, R. Burch and H. M. Coleman, *Appl. Catal. B.,* 2002, **39,** 65-74.

23 J. Llorca , P. Ramírez de la Piscina , J.-A. Dalmon and N. Homs, *Chem. Mater.*, 2004, **16,** 3573–3578.

24 V. A. D. O'Shea, N. Homs, E. B. Pereira, R. Nafria and P. Ramirez de la Piscina, *Catal. Today,* 2007, **126,** 148–152.

25 N. J. Divins, I. Angurell, C. Escudero, V. Pérez-Dieste and J. Llorca, *Science,* 2014, **346,** 620-623.

26 O. O. James, S. Maity, M. A. Mesubi, K. O. Ogunniran, T. O. Siyanbola, S. Sahu and R. Chaubey, *Green Chem.,* 2011, **13,** 2272−2284.

27 L. V. Mattos, G. Jacobs, B. H. Davis and F. b. B. Noronha, *Chem. Rev.,* 2012, **112,** 4094−4123.

28 J. Sun and Y. Wang, *ACS Catal.,* 2014, **4,** 1078-1090.

29 D. Zanchet, J. B. O. Santos, S. Damyanova, J. M. R. Gallo and J. M. C. Bueno, *ACS Catal.,* 2015, **5,** 3841−3863.

30 J. Lin, L. Chen, C. K. S. Choong, Z. Zhong and L. Huang, *Sci. China Chem.,* 2015, **58,** 60-78.

31 C. T. Campbell, *Nature Chem.,* 2012, **4,** 597-598.

32 F. Mariño, M. Boveri, G. Baronetti and M. Laborde, *Int. J. Hydrogen Energy,* 2001, **26,** 665-668.

33 P. Y. Sheng, W. W. Chiu, A. Yee, S. J. Morrison and H. Idriss, *Catal. Today,* 2007, **129,** 313-321.

34 J. Kugai, V. Subramani, C. Song, M. H. Engelhard and Y.-H. Chin, *J. Catal.,* 2006, **238,** 430-440.

35 M. Scott, M. Goeffroy, W. Chiu, M. A. Blackford and H. Idriss, *Top. Catal.,* 2008, **51,** 13-21.

36 H. Idriss, M. Scott, J. Llorca, S. C. Chan, W. Chiu, P.-Y. Sheng, A. Yee, M. A. Blackford, S. J. Pas, A. J. Hill, F. M. Alamgir, R. Rettew, C. Petersburg, S. D. Senanayake and M. A. Barteau, *ChemSusChem,* 2008, **1,** 905-910.

37 A. Simson, E. Waterman, R. Farrauto and M. Castaldi, *Appl. Catal. B.,* 2009, **89,** 58-64.

38 L. Chen, C. Choong, Z. Zhong, L. Huang, T. P. Ang, L. Hong and J. Lin, *J. Catal.,* 2010, **276,** 197-200.

39 A. Simson, R. Farrauto and M. Castaldi, *Appl. Catal. B.,* 2011, **106,** 295-303.

40 L. Huang, C. Choong, L. Chen, Z. Wang, Z. Zhong, C. Campos-Cuerva and J. Lin. *ChemCatChem,* 2013, **5,** 220-234.

41 F. Auprêtre, C. Descorme, D. Duprez, D. Casanave and D. Uzio, *J. Catal.,* 2005, **233,** 464-477.

42 R. M. Navarro, M. C. Alvarez-Galvân and M. C. Sânchez-Sânchez, *Appl. Catal. B.,* 2005, **55,** 229-241.

43 M. C. Sânchez-Sânchez, R. M. Navarro and J. L. G. Fierro, *Int. J. Hydrogen Energy,* 2007, **32,** 1462-1471.

44 A. Denis, W. Grzegorczyk, W. Gac and A. Machocki, *Catal. Today,* 2008, **137,** 453-459.

45 F. Frusteri, S. Freni, L. Spadaro, V. Chiodo, G. Bonura, S. Donato and S. Cavallaro, *Catal. Commun.,* 2004, **5,** 611-615.

46 H.-S. Roh, Y. Wang and D. L. King, *Top. Catal.,* 2008, **49,** 32-37.

47 J. Llorca, N. Homs, J. Sales and P. Ramirez de la Piscina, *J. Catal.,* 2002, **209,** 306-317.

48 Z. He, M. Yang, X. Wang, Z. Zhao and A. Duan, *Catal. Today,* 2012, **194,** 2– 8.

49 W. Cai, F. Wang, E. Zhan, A. C. Van Veen, C. Mirodatos and W. Shen, *J. Catal.*, 2008, **257,** 96-107.

50 H. Wang, Y. Liu, L. Wang and Y. N. Qin, *Chem. Eng. J.,* 2008, **145,** 25-31.

51 H. Idriss, *Platinum Met. Rev.,* 2004, **48,** 105-115.

52 T. X. T. Sayle, S. C. Parker and C. R. A. Catlow, *Surf. Sci.,* 1994, **316,** 329-336.

53 N. Kamiuchi, M. Haneda and M. Ozawa, *Catal. Today,* 2013, **201,** 79-84.

54 C. Diagne, H. Idriss and A. Kiennemann, *Catal. Commun.,* 2002, **3,** 565-571.

55 A. M. Karim, Y. Su, J. Sun, C. Yang, J. J. Strohm, D. L. King and Y. Wang, *Appl. Catal. B.,* 2010, **96,** 441-448.

56 W.-C. Chiu, R.-F. Horng and H.-M. Chou, *Int. J. Hydrogen Energy,* 2013, **38,** 2760-2769.

57 N. Palmeri, S. Cavallaro, V. Chioda, S. Freni, F. Frusteri and J. C. J. Bart, *Int. J. Hydrogen Energy,* 2007, **32,** 3335-3342.

58 T. Montini, L. De Rogatis, V. Gombac, P. Fornasiero and M. Graziani, *Appl. Catal. B.,* 2007, **71,** 125-134.

59 A. Birot, F. Epron, C. Descorme and D. Duprez, *Appl. Catal. B.,* 2008, **79,** 17-25.

60 Z. Zhong, H. Ang, C. Choong, L. Chen, L. Huang and J. Lin, *Phys. Chem. Chem. Phys.,* 2009, **11,** 872-880.

61 X. Wu and S. Kawi, *Energy. Environ. Sci.,* 2010, **3,** 334-342.

62 A. M. da Silva, K. R. de Souza, G. Jacobs, U. M. Graham, B. H. Davis, L. V. Mattos and F. B. Noronha, *Appl. Catal. B.,* 2011, **102,** 94-109.

63 J. S. Moura, M. O. G. Souza, J. D. A. Bellido, E. M. Assaf, M. Opportus, P. Reyes and M. do Carmo Rangel, *Int. J. Hydrogen Energy,* 2012, **37,** 3213-3224.

64 Y. Ando, K. Matsuoka, H. Takagi and K. Kuramoto, *Bull. Chem. Soc. Jpn.,* 2012, **85,** 517-521.

65 O. A. González Vargas, J. A. de los Reyes Heredia, J. A. Wang, L. F. Chen, A. Montesinos Castellanos and M. E. Llanos, *Int. J. Hydrogen Energy,* 2013, **38,** 13914-13925.

66 M. Bilal and S. D. Jackson, *Catal. Sci. Technol.,* 2013, **3,** 754-766.

67 D. V. Andreev, V. V. Radaev, L. L. Makarshin, A. G. Gribovskii, V. I. Zaikovskii and V. N. Parmon, *Kinet. Catal.,* 2014, **55,** 798-808.

68 L. Coronel, J. F. Múnera, A. M. Tarditi, M. S. Moreno and L. M. Cornaglia, *Appl. Catal. B.,* 2014, **160-161,** 254-266.

69 T. Hou, B. Yu, S. Zhang, T. Xu, D. Wang and W. Cai, *Catal. Commun.,* 2015, **58,** 137-140.

70 C. Diagne, H. Idriss and A. Kiennemann, *Catal. Commun.,* 2002, **3,** 565-571.

71 R. W. McCabe and P. J. Mltchell, *Ind. Eng. Chem. Prod. Res. Dev.,* 1984, **23,** 196-202.

72 M. Kourtelesis, P. Panagiotopoulou, S. Ladas and X. E. Verykios, *Top. Catal.,* 2015, **58,** 1202-1217.

73 J. J. F. Scholten, P. Mars, P. G. Menon and R. van Hardereld, Proceedings of the 3rd International Congress on Catalysis, Amsterdam, July 1964, Vol. 2, p. 881, North-Holland, 1965.

74 T. Shido, K. Asakura and Y. Iwasawa, *J. Catal.,* 1990, **122,** 55-67.

75 K. Tanabe, M. Misono, Y. Ono and H. Hattori, *Stud. Surf. Sci. Catal.,* 1989, **51,** 27-127.

76 A. Carrero , J. A. Calles, A. J. Vizcaíno, *Appl. Catal. A.,* 2007, **327,** 82–94.

77 M. Mavrikakis and M. A. Barteau, *J. Mol. Catal. A.,* 1998, **131,** 135-147.

78 H.-L. Chen, S.-H. Liu and J.-J. Ho, *J. Phys. Chem. B,* 2006, **110,** 14816-14823.

79 J. Zhang, Z. Zhong, X.-M. Cao, P. Hu, M. B. Sullivan and L. Chen, *ACS Catal.,* 2014, **4,** 448-456.

80 C. Houtman and M. A. Barteau, *J. Phys. Chem.,* 1991, **95,** 3155-3164.

81 H. Song, X. Bao, C. M. Hadad and U. S. Ozkan, *Catal. Lett.,* 2011, **141,** 43–54.

82 J. Sun, H. Zhang, N. Yu, S. Davidson and Y. Wang, *ChemCatChem,* 2015, **7,** 2932–2936.

83 P. Panagiotopoulou and D. Kondarides, *Catal. Today,* 2006, **112,** 49-52.

84 S. Bernal, J. J. Calvino, G. A. Cifredo, J. M. Gatica, J. A. Pérez Omil, A. Laachir and V. Perrichon, *Stud. Surf. Sci. Catal.,* 1995, **96,** 419-429.

85 D. I. Kondaride and X. E. Verykios, *J. Catal.,* 1998, **174,** 52-64.

86 C. Force, J. P. Belzunegui, J. Sanz, A. Martinez-Arias and J. Soria, *J. Catal.,* 2001, **197,** 192-199.

87 F. Fajardie, J.-F. Tempere, J.-M. Manoli, G. D. Mariadassou and G. Blanchard, *J. Chem. Soc. Faraday Trans.,* 1998, **94,** 3727-3735.

88 H. Song, L. Zhang, R. B. Watson, D. Braden and U. S. Ozkan, *Catal. Today,* 2007, **129,** 346-354.

89 W. Wang and Y. Q. Wang, *Int. J. Energy Res.,* 2008, **32,** 1432-1443.

90 L. Hernández and V. Kafarov, *J. Power Sources,* 2009, **192,** 195-199.

91 S. Yuvaraj, F.-Y. Lin, T.-H. Chang and C.-T. Yeh, *J. Phys. Chem. B,* 2003, **107,** 1044-1047.

92 A. Trovarelli, G. Dolcetti, C. de Leitenburg, J. Kašpar, P. Finetti and A. Santoni, *J. Chem. Soc. Faraday Trans.,* 1992, **88,** 1311-1319.

93 E. Ruchenstein and H. Y. Wang, *J. Catal.,* 2000, **190,** 32-38.

94 J. Von Hoene, R. G. Charles and W. M. Hickam, *J. Phys. Chem.,* 1958, **62,** 1098-1101.

95 S. Poston and A. Reisman. *J. Electron. Mater.,* 1988, **17,** 57-61.

96 J. A. Nario, M. Macias, F. J. Marchena and C. Real, *Stud. Surf. Sci. Catal.,* 1992, **72,** 423-433.

97 A. Théolier, A. K. Smith, M. Leconte, J. M. Basset, G. M. Zanderighi, R. Psaro and R. Ugo, *J. Organomet. Chem.,* 1980, **191,** 415-424.

98 X. Yu, F. Li, X. Ye and X. Xin, *J. Am. Ceram. Soc.,* 2000, **83,** 964–66.

99 A. Roman and B. Delmon, *J. Catal.,* 1973, **30,** 333-342.

100 P. Turlier, H. Praliaud, P. Moral, G. A. Martin and J. A. Dalmon, *Appl. Catal.,* 1985, **19,** 287-300.

101 B. Mile, D. Stirling, M. A. Zammitt, A. Lovell and M. Webb, *J. Catal.,* 1988, **114,** 217-229.

102 J. Z. Shyu, K. Otto, W. L. H. Watkins, G. W. Graham and R. K. Belitz, *J. Catal.,* 1988, **114,** 23-33.

103 A. Trovarelli, C. de Leitenburg, M. Boaro and G. Dolcetti, *Catal. Today,* 1999, **50,** 353-367.

104 D. Briggs and M. P. Seah, *Practical Surface Analysis, Vol. 1 : Auger and X-Ray Photoelectron Spectroscopy,* Wiley, New York, 1990.

105 D. I. Kondarides and X. E. Verykios, *J. Catal.,* 1998, **174,** 52-64.

106 R. Herrmann, M. Rennhak and A. Reller, *Beilstein J. Nanotechnol.*, 2014, **5,** 2413–2423.

107 C. M. Y. Yeung, K. M. K. Yu, Q. J. Fu, D. Thompsett, M. I. Petch and S. C. Tsan, *J. Am. Chem. Soc.,* 2005, **127,** 18010-18011.

108 S. Tuti and F. Pepe, *Catal. Lett.,* 2008, **122,** 196–203.

109 M. P. Hyman and J. M. Vohs, *Surf. Sci.*, 2011, **605,** 383-389.

110 A. R. Passos, L. Martins, S. H. Pulcinelli, C. V. Santilli and V. Briois, *Catal. Today*, 2014, **229,** 88-94.

111 A. M. Karim, Y. Su, M. H. Engelhard, D. L. King and Y. Wang, *ACS Catal.,* 2011, **1,** 279-286.

112 J. Suna, A. M. Karim, D. Meib, M. Engelhard, X. Bao and Y. Wang, *Appl. Catal. B.,* 2015, **162,** 141–148.

113 F. Haga, T. Nakajima, H. Miya and S. Mishima, *Catal. Lett.,* 1997, **48,** 223-227.

114 J. R. Mielenz, *Curr. Opin. Microbiol.,* 2001, **4,** 324-329.

115 J. Llorca, P. Ramirez de la Piscina, J. A. Dalmon, J. Sales and N. Homs, *Appl. Catal. B.,* 2003, **43,** 355-369.

116 M. S. Batista, R. K. S. Santos, E. M. Assaf, J. M. Assaf and E. A. Ticiasnelli, *J. Power Sources,* 2003, **124,** 99-103.

117 H. Song, L. Z. Zhang and U. S. Ozkan, *Green Chem.,* 2007, **9,** 686-694.

118 S. S. Y. Lin, D. H. Kim and S. Y. Ha, *Catal. Lett.,* 2008, **122,** 295-301.

119 A. Simson, S. G. Podkolzin and M. J. Castaldi, presented in part at 23rd North American Catalysis Society Meeting, P- W-BRC-39, Louisville, June, 2013.

Graphical and Textual Abstract

Oxide-supported Rh catalysts for H_2 generation from low-temperature ethanol steam reforming: Effects of support, Rh precursor and Rh loading on catalytic performance

Lin Huang, Catherine Choong, Luwei Chen, Zhan Wang, Ziyi Zhong, Kee Ann Chng and Jianyi Lin

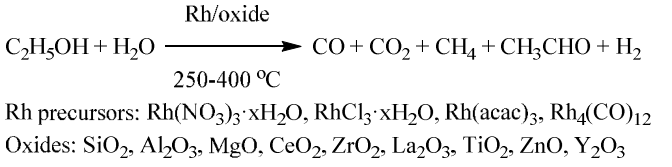

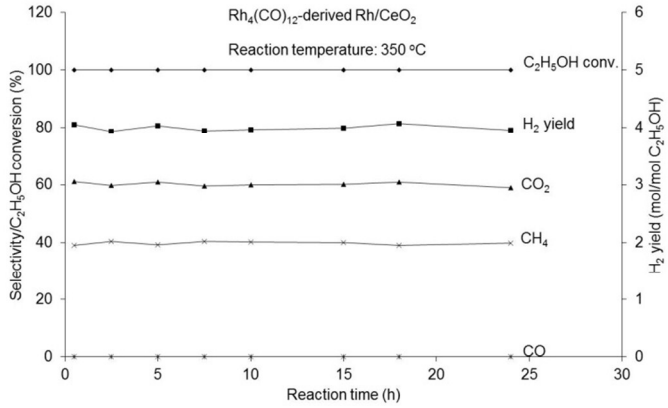

$Rh_4(CO)_{12}$-derived Rh/CeO_2 is superior to the other oxide-supported Rh catalysts. Coking is the only cause of catalyst deactivation which affects the catalytic stability of Rh/CeO_2. Both CeO_2-supported Rh^0 and Rh^+ may participate in catalysis for ESR.